# Vector Solitons and Their Internal Oscillations in Birefringent Nonlinear Optical Fibers*

*By Jianke Yang*

In this article, the vector solitons in birefringent nonlinear optical fibers are studied first. Special attention is given to the single-hump vector solitons due to evidences that only they are stable. Questions such as the existence, uniqueness, and total number of these solitons are addressed. It is found that the total number of them is continuously infinite and their polarizations can be arbitrary. Next, the internal oscillations of these vector solitons are investigated by the linearization method. Discrete eigenmodes of the linearized equations are identified. Such modes cause to the vector solitons a kind of permanent internal oscillations, which visually appear to be a combination of translational and width oscillations in the A and B pulses. The numerically observed radiation shelf at the tails of interacting pulses is also explained. Finally, the asymptotic states of the perturbed vector solitons are studied within both the linear and nonlinear theory. It is found that the state of internal oscillations of a vector soliton is always unstable. It invariably emits energy radiation and eventually evolves into a single-hump vector soliton state.

Address for correspondence: Department of Mathematics and Statistics, The University of Vermont, 16 Colchester Avenue, Burlington, VT 05401. E-mail: jyang@emba.uvm.edu

* "Vector solitons" is a name researchers in nonlinear optics use for solitary waves in birefringent nonlinear optical fibers. They are not solitons in a strict mathematical sense, but are nevertheless shape preserving.

*STUDIES IN APPLIED MATHEMATICS* 98:61–97


Published by Blackwell Publishers, 350 Main Street, Malden, MA 02148, USA, and 108 Cowley Road, Oxford, OX4 1JF, UK.

## 1. Introduction

The idea of using solitons as information bits in a high-data-rate telecommunication system was first proposed by Hasegawa and Tappert [1] in 1973. Since then, a great deal of experimental and theoretical work has been done on the pulse propagation in a nonlinear optical fiber. The early theoretical work took the nonlinear Schrödinger equation (NLS) as the underlying mathematical model, and the propagation of solitonian pulses have all the nice properties associated with the integrable NLS equation. Menyuk [3] first realized the importance of birefringence in an optical fiber and studied its effects on the pulse propagation. Birefringence can lead to pulse splitting, which is not desirable in communication applications. This effect may be balanced by nonlinearity in the fiber since nonlinearity tends to hold pulses together. When all these effects (birefringence, nonlinearity, linear dispersion, etc.) are taken into consideration, a multiple-scale perturbation analysis can be employed to obtain the evolution equations of pulses in a birefringent nonlinear optical fiber. This has been done by Menyuk [3]. After some simplifications, the equations can be written as

$$iA_t + A_{xx} + (|A|^2 + \beta|B|^2)A = 0, \tag{1.1a}$$

$$iB_t + B_{xx} + (|B|^2 + \beta|A|^2)B = 0, \tag{1.1b}$$

where $A$ and $B$ represent the complex amplitudes of the two polarization components, and $\beta$ is a real-valued cross-phase modulation coefficient. The system (1.1) is integrable only when $\beta$ is equal to 0 or 1. But for most optical fibers, $\beta$ is not equal to 0 or 1. This destroys integrability and complicates the pulse evolution behaviors. For instance, vector solitons still exist in the system (1.1), but when they collide, they may merge into a single soliton, destroy each other, or be reflected back by each other. A certain amount of energy radiation is also emitted when collision takes place [4, 5]. Additionally, vector solitons, when perturbed, undergo complicated internal oscillations and shed radiation [6].

Vector solitons in the system (1.1), although not as robust as those associated with an integrable system, still play an important role in the solution evolution. They have been investigated by Mesentsev and Turitsyn [7], Kaup et al. [8], Haelterman and Sheppard [9], Silberberg and Barad [10], and Yang and Benney [5]. Mesentsev and Turitsyn proved the stability of the vector solitons of equal amplitudes by constructing a Lyapunov function for the Hamiltonian associated with Equations (1.1). Kaup et al. studied the internal dynamics of vector solitons by the variational principle method. They approximated the vector solitons by a Gaussian ansatz, inserted it into the Lagrangian density, and then obtained a system of ordinary differential

equations (o.d.e.) for the evolution of the ansatz parameters. They found a continuous family of fixed points of the o.d.e. system, which represent symmetric vector solitons with an arbitrary polarization. They also showed that these vector soliton solutions are stable by examining the linear stability of those fixed points. Haelterman and Sheppard's results confirmed the existence of these vector solitons. Silberberg and Barad identified two families of vector solitons, one symmetric and the other one antisymmetric. They also showed numerically that only the symmetric family of solutions are stable. In joint work with D. Benney, we studied the same problem. We found, by a numerical approach, infinite families of vector solitons. Only one of these families is single-humped and symmetric, and it corresponds to the one found by Kaup et al. All other families of solutions are multi-humped. On the basis of some analytical results and numerical evidence, we conjectured that only the single-humped vector solitons are stable.

The internal oscillations of vector solitons is a complicated process. This problem has been studied by Ueda and Kath [6] and Kaup et al. [8] using the variational principle method. Ueda and Kath assumed the spatial shapes of the pulses to take the form of the NLS solitons with frequency chirping, but allowed the shape parameters such as pulse position and width to evolve with time. Inserting the NLS solitons into the Lagrangian density and taking variations with respect to each pulse parameter, they derived a system of ordinary differential equations which govern the evolution of the shape parameters. They identified two types of internal oscillations (translational oscillation and pulse-width oscillation) and determined their frequencies. They also showed that there is a transfer of energy between these two types of oscillations, which results in the inelastic nature of the soliton collisions. Kaup et al. used the same variational principle method except they approximated the pulses by a Gaussian ansatz. This oversimple approximation enabled them to solve all the necessary integrals involved in their analysis. They found a continuous family of stationary solutions, which represent vector solitons with an arbitrary polarization. Examining small internal vibrations of these vector solitons, they found three oscillational eigenmodes; two were those found by Ueda and Kath and one was new.

The analytical models by Ueda and Kath and Kaup et al. can qualitatively describe some aspects of the vector solitons' internal dynamics over short time scales. The major drawback of their models is that radiation was not considered. It is well known that radiation is one of the key players in the internal dynamics of vector solitons. Radiation carries energy away from the dominant pulses and has a damping effect on them. In particular, low-wavenumber radiation has been observed numerically as a low shelf at the tails of the oscillating pulses. Such radiation propagates at velocities close to that of the vector soliton and therefore remains close to the pulses and affects their dynamics over long time scales. Clearly the exclusion of radiation

in an analytical model will make its predictions invalid over long time scales. Another drawback of their models is that they limited the evolution of the pulse shape to the ansatz chosen, so shape changes cannot go beyond those modeled by changes in the shape parameters. The true pulse shape and its evolution are still unclear.

In this article, the problem of vector solitons and their internal oscillations is revisited. First, we address the existence, uniqueness, and total number of (stable) single-hump vector solitons. Next, we study the internal oscillations of vector solitons with radiation included. The linearization and perturbation methods are used. The oscillational eigenmodes found by Ueda and Kath and Kaup et al. are reconsidered and their true natures clarified. The true pulse shape in the internal oscillations is determined. Predictions on the long-time-pulse dynamics are also given. The results obtained provide a clear and complete picture of the internal dynamics of vector solitons.

## 2. Vector solitons

It has been known that vector solitons of the form

$$A = e^{i\omega_1 t}\, r_1(x), \tag{2.1a}$$

$$B = e^{i\omega_2 t}\, r_2(x) \tag{2.1b}$$

exist in the system (1.1), in which case $r_1$ and $r_2$ satisfy the equations

$$r_{1xx} - \omega_1 r_1 + (r_1^2 + \beta r_2^2) r_1 = 0, \tag{2.2a}$$

$$r_{2xx} - \omega_2 r_2 + (r_2^2 + \beta r_1^2) r_2 = 0. \tag{2.2b}$$

We are interested only in the solitary waves that exponentially decay as $|x| \to \infty$, so it is necessary that $\omega_1, \omega_2 > 0$. For convenience, we take $\omega_1 = 1$. This can always be achieved by a rescaling of variables $r_1, r_2$, and $x$. We further denote $\omega_2$ as $\omega$. Equations (2.2) have a great number of solutions for any value of $\beta$ (see [5]). The degenerate solutions, in which one of $r_1$ and $r_2$ is equal to zero, is easy to determine. For instance, if $r_2 = 0$, then

$$r_1 = \sqrt{2}\,\mathrm{sech}\, x. \tag{2.3}$$

These degenerate solutions are always stable for any value of $\beta$. In the rest of this section only the nondegenerate solutions are discussed. These solutions are generally hard to determine analytically, but can be effectively found numerically. Some of the single-hump solutions (in both $r_1$ and $r_2$) for $\beta = \frac{2}{3}$ are illustrated in Figure 1. They are symmetric in $x$ and centered together with the center being their common maximum point. Some multi-hump solutions for $\beta = \frac{2}{3}$ and vector solitons for other values of $\beta$ can be found

in [5]. Evidence in [5] shows that when $\beta > 0$, the single-hump solutions are stable while the multi-hump ones are not; when $\beta < 0$, both the single and multi-hump solutions are unstable. So, in the following, we focus on the single-hump solutions for $\beta > 0$.

As is clear from Figure 1, the polarizations of the single-hump solutions $r_2(0)/r_1(0)$ change continuously with $\omega$. At one extreme where $r_2 \ll r_1$, $r_2$ is called a daughter wave or a shadow. In this case, $\omega$ is found to be [5]

$$\omega = \omega_{\mathrm{I}} \equiv \frac{(\sqrt{1+8\beta}-1)^2}{4}. \tag{2.4}$$

At the other extreme where $r_1 \ll r_2$, it is found that

$$\omega = \omega_{\mathrm{II}} \equiv \frac{4}{(\sqrt{1+8\beta}-1)^2}. \tag{2.5}$$

Single-hump solutions exist when $\omega$ is in the interval $(\omega_{\mathrm{I}}, \omega_{\mathrm{II}})$. This interval against $\beta$ is illustrated in Figure 2. When $\omega$ is in this range, single-hump solutions $r_1$ and $r_2$ exist.

The value $\beta = 1$ is quite special in Figure 2. When $\beta = 1$, the interval $(\omega_{\mathrm{I}}, \omega_{\mathrm{II}})$ shrinks to the point 1, which means that single-hump solutions exist only when $\omega = 1$. This result is confirmed in [5] and [11]. Furthermore, the vector solitons for $\omega \neq 1$ were explicitly given in [11] and they are all multi-hump solutions.

Next we discuss the uniqueness and total number of single-hump vector solitons for positive $\beta$. When $\beta = 1$, single-hump solutions $r_1$ and $r_2$ exist if $\omega = 1$. These solutions are

$$r_1 = \sqrt{2}\cos\alpha \operatorname{sech} x, \qquad r_2 = \sqrt{2}\sin\alpha \operatorname{sech} x, \tag{2.6}$$

where $\alpha$ is a free parameter. Note that the polarizations of these solutions $r_2(0)/r_1(0)$ can be arbitrary and the number of them is continuously infinite. When $\beta \neq 1$, single-hump solutions exist when $\omega$ is in the interval $(\omega_{\mathrm{I}}, \omega_{\mathrm{II}})$ specified above (also see Figure 2). If $\omega$ is close to the boundary value $\omega_{\mathrm{I}}$ or $\omega_{\mathrm{II}}$, then $r_2 \ll r_1$ or $r_1 \ll r_2$, and the solution is a wave and daughter-wave structure. In this case, it is easy to show by perturbation methods that single-hump solutions are unique if $\omega$ is given. If $\omega$ is not close to those boundary values, it is reasonable to conjecture that single-hump solutions are still unique. This is confirmed by our numerical results. As $\omega$ varies continuously from $\omega_{\mathrm{I}}$ to $\omega_{\mathrm{II}}$, the polarization of $r_2(0)/r_1(0)$ changes continuously from 0 to $\infty$ (see Figure 1). So when $\beta \neq 1$, the number of single-hump solutions is still continuously infinite, and the polarizations of them can also be arbitrary, just as the case with $\beta = 1$.

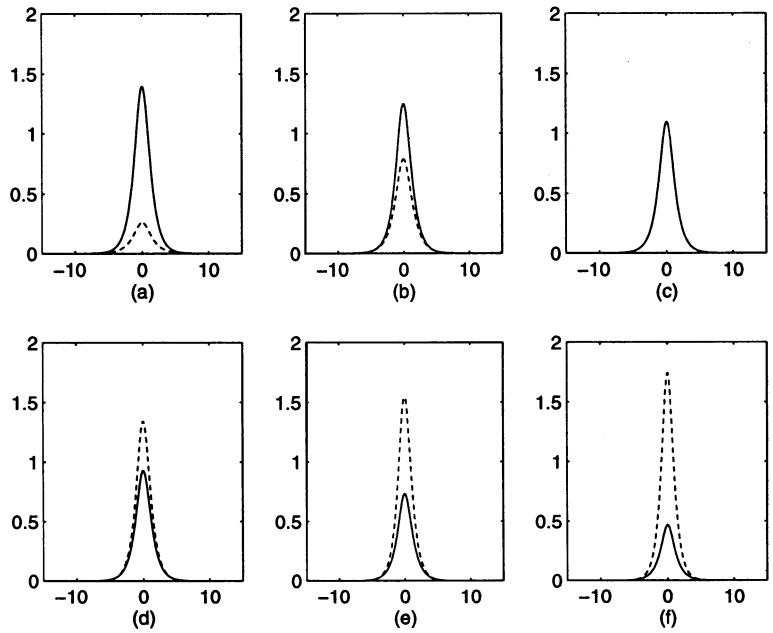


Figure 1. Some of the single-hump $(r_1, r_2)$ solutions in Equations (2.2) with $\beta = \frac{2}{3}$. The value of $\omega$ is (a) 0.6; (b) 0.8; (c) 1; (d) 1.2; (e) 1.4; (f) 1.6. Solid curves, $r_1$; dashed curves, $r_2$.

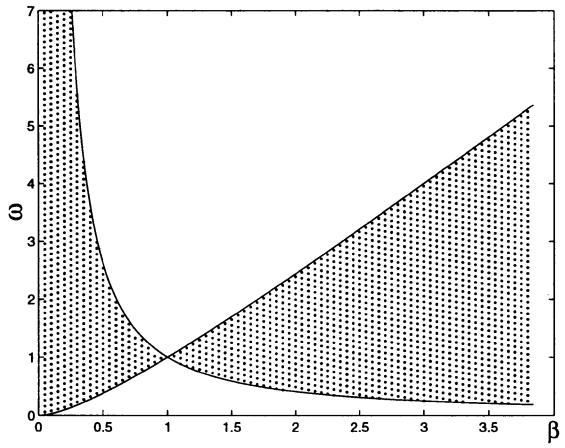


Figure 2. The $(\omega,\ \beta)$ region (shaded) where single-hump solutions exist in Equations (2.2). The two boundary curves are given by (2.4) and (2.5).

### 3. Internal oscillations of vector solitons

When vector solitons (2.1) are disturbed, they undergo complicated internal oscillations. For instance, if the two polarization components of a vector soliton are spatially separated, they trap each other and form a bound state (see Figure 3). In this state their widths dilate and contract and their central positions oscillate about one another. Some amount of radiation is also emitted in the oscillation process. Radiation carries energy away from the vector soliton and leads to its degradation. In some cases low-wavenumber radiation is observed numerically as a low shelf at the tails of the oscillating pulses [6]. Such radiation propagates at velocities close to that of the vector soliton and therefore remains close to the pulses and affects their dynamics over long time scales.

In this section, we study the internal oscillations of single-hump vector solitons (2.1) by the linearization method. Without loss of generality, we take $\omega_1 = 1$ and denote $\omega_2$ as $\omega$. It is known from the previous section that when $\omega$ falls in the interval $(\omega_{\mathrm{I}}, \omega_{\mathrm{II}})$ as illustrated in Figure 2, single-hump vector

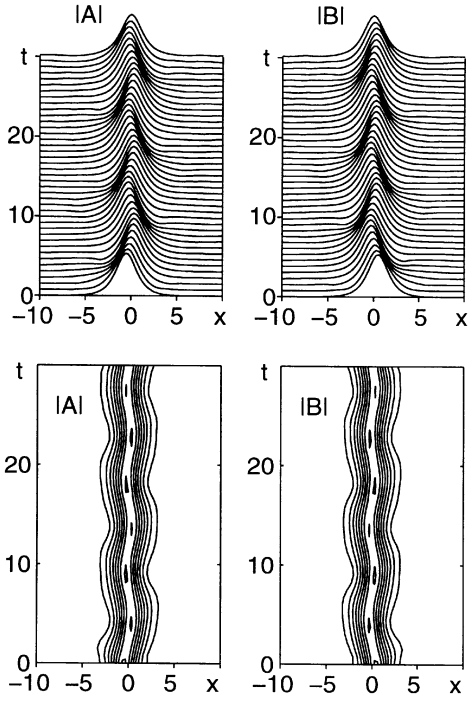


Figure 3. Internal oscillations of a vector soliton in Equations (1.1). The initial condition is $A(x,0) = \sqrt{2/(1+\beta)}\,\mathrm{sech}(x+0.5)$, $B(x,0) = \sqrt{2/(1+\beta)}\,\mathrm{sech}(x-0.5)$, and $\beta = 0.2$. The top two graphs are the amplitude plots, and the bottom two are the contour plots. Contours are evenly spaced at 0.2:0.15:1.25 for both $|A|$ and $|B|$.

solitons exist. Furthermore, they are unique when $\beta \neq 1$. Suppose now that (2.1) is perturbed. Then

$$A = e^{it}\{r_1(x) + \tilde{A}(x,t)\}, \tag{3.1a}$$

$$B = e^{i\omega t}\{r_2(x) + \tilde{B}(x,t)\}, \tag{3.1b}$$

where $\tilde{A}$ and $\tilde{B}$ are disturbances and are assumed small. When (3.1) is substituted into Equations (1.1) and higher-order terms neglected, the following linear equations are obtained for $\tilde{A}$ and $\tilde{B}$:

$$i\tilde{A}_t - \tilde{A} + \tilde{A}_{xx} + (2r_1^2 + \beta r_2^2)\tilde{A} + r_1^2\tilde{A}^* + \beta r_1 r_2(\tilde{B} + \tilde{B}^*) = 0, \tag{3.2a}$$

$$i\tilde{B}_t - \omega\tilde{B} + \tilde{B}_{xx} + (2r_2^2 + \beta r_1^2)\tilde{B} + r_2^2\tilde{B}^* + \beta r_1 r_2(\tilde{A} + \tilde{A}^*) = 0. \tag{3.2b}$$

In the remainder of this section we first determine all the eigenmodes of the above linear equations; then we solve them for an arbitrary initial condition $\tilde{A}(x,0)$ and $\tilde{B}(x,0)$.

### *3.1. Linearization analysis for vector solitons of equal amplitudes*

The vector soliton of equal amplitudes is

$$r_1(x) = r_2(x) = \sqrt{2/(1+\beta)}\,\operatorname{sech} x, \tag{3.3}$$

with $\omega = 1$. For this soliton, Equations (3.2) can be simplified. We define the new variables

$$u = \tilde{A} + \tilde{B}, \qquad v = \tilde{A} - \tilde{B}; \tag{3.4}$$

then the equations for $u$ and $v$ are decoupled. These equations are

$$iu_t + u_{xx} - u + 4\operatorname{sech}^2 x u + 2\operatorname{sech}^2 x u^* = 0, \tag{3.5}$$

$$iv_t + v_{xx} - v + \frac{4}{1+\beta}\operatorname{sech}^2 x v + \frac{2(1-\beta)}{1+\beta}\operatorname{sech}^2 x v^* = 0. \tag{3.6}$$

Note that Equation (3.5) is also the linearized equation of NLS around its soliton, while Equation (3.6) is new. Next, we solve these two equations.

3.1.1. *Solution of Equation* (3.5). It is convenient to work with the variables $u$ and $u^*$. We denote $U = (u, u^*)^{\mathrm{T}}$, where the superscript T represents the transpose. Then, $U$ satisfies the equation

$$iU_t + LU = 0, \tag{3.7}$$

where the linear operator $L$ is

$$L = \sigma_3(\partial_{xx} - 1) + 2\,\mathrm{sech}^2 x(2\sigma_3 + i\sigma_2), \tag{3.8}$$

and

$$\sigma_1 = \begin{pmatrix} 0 & 1 \\ 1 & 0 \end{pmatrix}, \qquad \sigma_2 = \begin{pmatrix} 0 & -i \\ i & 0 \end{pmatrix}, \qquad \sigma_3 = \begin{pmatrix} 1 & 0 \\ 0 & -1 \end{pmatrix} \tag{3.9}$$

are Pauli spin matrices. The eigenstates of Equation (3.7) are of the form

$$U(x, t) = e^{i\lambda t}\psi(x), \tag{3.10}$$

where

$$L\psi = \lambda\psi. \tag{3.11}$$

These states have been worked out by Kaup [12]. The eigensolutions in the continuous spectrum of $L$ are

$$\psi(x, k) = e^{ikx}\left(1 - \frac{2ik}{(k+i)^2}e^{-x}\,\mathrm{sech}\,x\right)\begin{pmatrix} 0 \\ 1 \end{pmatrix} + \frac{e^{ikx}\,\mathrm{sech}^2 x}{(k+i)^2}\begin{pmatrix} 1 \\ 1 \end{pmatrix} \tag{3.12}$$

with $\lambda_\psi = k^2 + 1$ and

$$\bar{\psi}(x, k) = \sigma_1\psi, \qquad \text{with } \lambda_{\bar{\psi}} = -(k^2 + 1). \tag{3.13}$$

The solutions in the discrete spectrum of $L$ are a linear combination of the two functions

$$\psi_e(x) = \mathrm{sech}\,x\begin{pmatrix} 1 \\ -1 \end{pmatrix}, \qquad \psi_0(x) = \mathrm{sech}\,x\tanh x\begin{pmatrix} 1 \\ 1 \end{pmatrix} \tag{3.14}$$

with the same eigenvalue $\lambda = 0$. Since $L$ is not self-adjoint, two more states,

$$\phi_e(x) = \mathrm{sech}\,x(x\tanh x - 1)\begin{pmatrix} 1 \\ 1 \end{pmatrix} \qquad \text{and} \qquad \phi_0(x) = x\psi_e \tag{3.15}$$

need to be included for closure. These two states are the generalized eigenstates and the $L$ operator acting on them gives

$$L\phi_e = -2\psi_e, \qquad L\phi_0 = -2\psi_0. \tag{3.16}$$

The discrete eigenstates $\psi_e, \psi_0, \phi_e$, and $\phi_0$, together with the continuous ones $\psi$ and $\bar{\psi}$, form a complete set [12]. To find the solution $U(x,t)$ for an arbitrary initial condition $U(x,0)$, we first expand $U(x,0)$ into these eigenstates as

$$U(x,0) = \int_{-\infty}^{\infty} \{c(k)\psi(x,k) + \bar{c}(k)\bar{\psi}(x,k)\}\, dk + c_e\psi_e(x) + c_0\psi_0(x) + d_e\phi_e(x) + d_0\phi_0(x), \tag{3.17}$$

where the coefficients can be determined by choosing an inner product and the orthogonal sets properly (see [12] for details). In particular, the coefficients in front of the discrete eigenstates are

$$c_e = -\frac{1}{2}\langle U(x,0), \phi_e\rangle, \qquad c_0 = \frac{1}{2}\,\langle U(x,0),\ \phi_0\rangle, \tag{3.18a}$$

$$d_e = -\frac{1}{2}\,\langle U(x,0),\ \psi_e\rangle, \qquad d_0 = \frac{1}{2}\,\langle U(x,0),\ \psi_0\rangle, \tag{3.18b}$$

where the inner product is defined as

$$\langle f, g\rangle = \int_{-\infty}^{\infty} f^{\mathrm{T}}\sigma_3\, g dx. \tag{3.19}$$

Then the solution $U(x,t)$ is

$$U(x,t) = \int_{-\infty}^{\infty} \{c(k)\psi(x,k)e^{i(k^2+1)t} + \bar{c}(k)\bar{\psi}(x,k)e^{-i(k^2+1)t}\}\, dk + c_e\psi_e(x) + c_0\psi_0(x) + d_e\{\phi_e(x) - 2it\psi_e(x)\} + d_0\{\phi_0(x) - 2it\psi_0(x)\}. \tag{3.20}$$

In view of the relation (3.1) and (3.4), it is easy to see that the last four terms in the solution $U(x,t)$ can be absorbed into the vector soliton (3.3). This absorption results in a phase, position, width, and velocity shift of (3.3) respectively. The integral in (3.20) is the collection of dispersive wave modes and is the radiation component of the $U(x,t)$ solution. It can cause the $A$ and $B$ pulses of the vector soliton (3.3) to dilate and contract simultaneously, just as radiation does in a perturbed NLS soliton. This in-phase width oscillation decays in proportion to $t^{-1/2}$, which is the well-known decay rate of linear dispersive waves. When compared to the results in [6] and [8], it appears that this transient in-phase width oscillation was accounted for in their analyses as a linear symmetric eigenmode for the parameters in the chosen ansatzes. This means that in their analyses radiation in $U(x,t)$ was treated as a nondecaying symmetric width oscillation. Next, we analyze the integral in (3.20) a little further. The dispersion relations of the wave modes in the integral are $\lambda = \pm(k^2+1)$, where $\lambda$ is the frequency and $k$ the far-field wavenumber of the

wave. When time is large, the only dominant modes in the vicinity of the vector soliton are those with group velocity $C_g = \pm 2k$ close to 0, i.e., $k \approx 0$ and $\lambda \approx \pm 1$. This indicates that in the solution $U(x, t)$, the radiation component near the vector soliton consists of mainly low-wavenumber wave modes that are oscillating at frequencies $\pm 1$ when time gets large. More specifically, for large $t$ and small or moderate $x$,

$$\int_{-\infty}^{\infty} \{c(k)\psi(x, k)e^{i(k^2+1)t} + \bar{c}(k)\bar{\psi}(x, k)e^{-i(k^2+1)t}\}\, dk$$
$$\longrightarrow \sqrt{\frac{\pi}{4t}}\, \{c(0)\psi(x, 0)e^{i(t+\pi/4)} + \bar{c}(0)\bar{\psi}(x, 0)e^{-i(t+\pi/4)}\}, \qquad t \to \infty. \tag{3.21}$$

Recall that the functions

$$\psi(x, 0) = \begin{pmatrix} -\operatorname{sech}^2 x \\ \tanh^2 x \end{pmatrix}, \qquad \bar{\psi}(x, 0) = \sigma_1 \psi(x, 0), \tag{3.22}$$

are even in $x$ and have a shelf in both $x$ directions, so, the integral (3.21) asymptotically becomes a symmetric low shelf at the tails of the vector soliton. This low shelf constitutes part of the radiation shelf, which has been observed numerically [6]. We discuss this problem further later in the article.

3.1.2. *Solution of Equation* (3.6). As before, we work with the variables $v$ and $v^*$ and denote $V = (v, v^*)^{\mathrm{T}}$. Then, $V$ satisfies the equation

$$iV_t + L_\beta V = 0, \tag{3.23}$$

where the linear operator $L_\beta$ is

$$L_\beta = \sigma_3(\partial_{xx} - 1) + 2\operatorname{sech}^2 x \left( \frac{2}{1+\beta}\sigma_3 + \frac{1-\beta}{1+\beta} i\sigma_2 \right). \tag{3.24}$$

The eigenstates of Equation (3.23) are

$$V(x, t) = e^{i\lambda t}\psi(x), \tag{3.25}$$

where

$$L_\beta \psi = \lambda \psi. \tag{3.26}$$

When $\beta = 0$, the operator $L_\beta$ becomes $L$, and its eigenstates are as given previously. When $\beta = 1$, $L_\beta$ becomes

$$L_1 = \sigma_3(\partial_{xx} - 1 + 2\operatorname{sech}^2 x). \tag{3.27}$$

In this case, $L_1$ has two discrete eigenfunctions

$$\psi_{1e} = \psi_e = \operatorname{sech} x \begin{pmatrix} 1 \\ -1 \end{pmatrix}, \qquad \phi_{1e} = \operatorname{sech} x \begin{pmatrix} 1 \\ 1 \end{pmatrix} \tag{3.28}$$

with the same eigenvalue $\lambda = 0$. The continuous spectrum of $L_1$ is $|\lambda| \geq 1$. For each $\lambda > 1$ or $\lambda < -1$, there are two linearly independent eigenfunctions. Let us denote them as $\psi_1^{(1)}(x, \lambda)$ and $\psi_1^{(2)}(x, \lambda)$. When $\lambda < -1$, these two functions are

$$\psi_1^{(1)} = \begin{pmatrix} f_1(x, \lambda) \\ 0 \end{pmatrix}, \qquad \psi_1^{(2)} = \begin{pmatrix} f_2(x, \lambda) \\ 0 \end{pmatrix}, \tag{3.29}$$

where $f_1$ and $f_2$ are the two linearly independent solutions of the Schrödinger equation

$$f_{xx} - (1 + \lambda) f + 2 \operatorname{sech}^2 x f = 0 \tag{3.30}$$

and can be expressed in terms of the hypergeometric functions [13]. When $\lambda > 1$,

$$\psi_1^{(1)}(x, \lambda) = \sigma_1 \psi_1^{(1)}(x, -\lambda), \qquad \psi_1^{(2)}(x, \lambda) = \sigma_1 \psi_1^{(2)}(x, -\lambda). \tag{3.31}$$

When $\lambda = 1$ or $-1$, there is only one eigenfunction $(\tanh x \ 0)^{\mathrm{T}}$ or $(0 \ \tanh x)^{\mathrm{T}}$. Since the operator $L_1$ is Hermitian, all these eigenstates form a complete set.

When $\beta$ continuously moves away from 0 to 1, the eigenstates of the operator $L_\beta$ change accordingly. First of all, the discrete eigenstate

$$\psi_{\beta e} = \psi_e = \operatorname{sech} x \begin{pmatrix} 1 \\ -1 \end{pmatrix} \tag{3.32}$$

with $\lambda = 0$ remains unchanged, but its generalized eigenstate becomes

$$\phi_{\beta e} = g(x, \beta) \begin{pmatrix} 1 \\ 1 \end{pmatrix}, \tag{3.33}$$

where $g(x, \beta)$ is the solution of the equation

$$g_{xx} - g + \frac{6 - 2\beta}{1 + \beta} \operatorname{sech}^2 x g = -2 \operatorname{sech} x. \tag{3.34}$$

The operator $L_\beta$ acting on $\phi_{\beta e}$ gives

$$L_\beta \phi_{\beta e} = -2 \psi_{\beta e}. \tag{3.35}$$

Equation (3.34) has a unique localized solution for $g$ if $\beta \neq 1$. This solution can be determined numerically. When $\beta = 0$,

$$g(x, 0) = \operatorname{sech} x (x \tanh x - 1). \tag{3.36}$$

As $\beta \to 1$, $g(x, \beta) \longrightarrow \operatorname{sech} x$ (when normalized so that $g(0, \beta) = 1$). Second, as $\beta$ moves away from 0, the discrete eigenstate $\psi_0$ (with $\lambda = 0$) and its generalized eigenstate $\phi_0$ split into two discrete eigenstates $\psi_{\beta 0}$ and $\bar{\psi}_{\beta 0}$ $(= \sigma_1 \psi_{\beta 0})$ with nonzero eigenvalues $\lambda_\beta$ $(> 0)$ and $-\lambda_\beta$ respectively. These states can be determined numerically using the shooting method. The dependence of $\lambda_\beta$ on $\beta$ is plotted in Figure 4. When $\beta$ is small, the perturbation analysis by this author and D. J. Benney [5] shows that to leading order, $\lambda_\beta \approx \sqrt{64\beta/15}$. Another result by Ueda and Kath [6] is also relevant here. As we show later in this article, the eigenstates $\psi_{\beta 0}$ and $\bar{\psi}_{\beta 0}$ cause to the vector soliton (3.3) a kind of internal oscillation that looks like a combination of translational and width oscillations discussed in [6]. Ueda and Kath showed that the frequency of the translational oscillation (when adjusted to the present context) is $\sqrt{64\beta/[15(1+\beta)]}$ for small $\beta$. This result is also plotted in Figure 4 for comparison. Evidently, for small $\beta$, these three curves agree well. For moderate $\beta$, differences between them become manifest. Three typical eigenfunctions $\psi_{\beta 0}$ with $\beta = 0.05$, 0.2, and $\frac{2}{3}$ are plotted in Figure 5. These functions have been normalized so that the maximum value of $|\psi_{\beta 0}[2]|$ is equal to 1. As $\beta$ moves from 0 to 1, so does $\lambda_\beta$. Meanwhile, the relative size of $\psi_{\beta 0}[1]$ gets smaller, and $\psi_{\beta 0}[2]$ gets flatter. When $\beta \to 1^-$, these two discrete eigenstates $\psi_{\beta 0}$ and $\bar{\psi}_{\beta 0}$ degenerate into the continuous eigenstates $(0 \quad \tanh x)^{\mathrm{T}}$ and $(\tanh x \quad 0)^{\mathrm{T}}$ with $\lambda = 1$ and $-1$ respectively.

The continuous spectrum of the operator $L_\beta$ for $0 < \beta < 1$ is $|\lambda| > 1$. For each eigenvalue in this range, there are two linearly independent eigenfunctions, which we denote as $\psi_\beta^{(1)}(x, \lambda)$ and $\psi_\beta^{(2)}(x, \lambda)$. Note that

$$\psi_\beta^{(1)}(x, -\lambda) = \sigma_1 \psi_\beta^{(1)}(x, \lambda), \qquad \psi_\beta^{(2)}(x, -\lambda) = \sigma_1 \psi_\beta^{(2)}(x, \lambda). \tag{3.37}$$

These eigenfunctions can be effectively determined by the shooting method.

The discrete and continuous eigenstates of the operator $L_\beta$ as described above also form a complete set. Directly proving their completeness may be difficult. But the study we just conducted on the changes of the eigenstates of

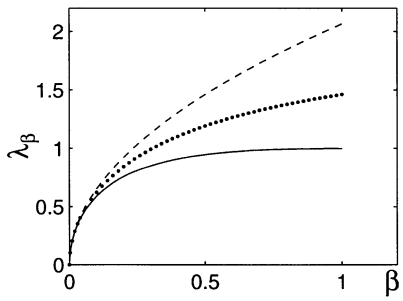


Figure 4. Dependence of the operator $L_\beta$'s discrete eigenvalue $\lambda_\beta$ on $\beta$ (solid curve). The dashed curve is $\lambda = \sqrt{64\beta/15}$, and the dotted curve is $\lambda = \sqrt{64\beta/[15(1+\beta)]}$.

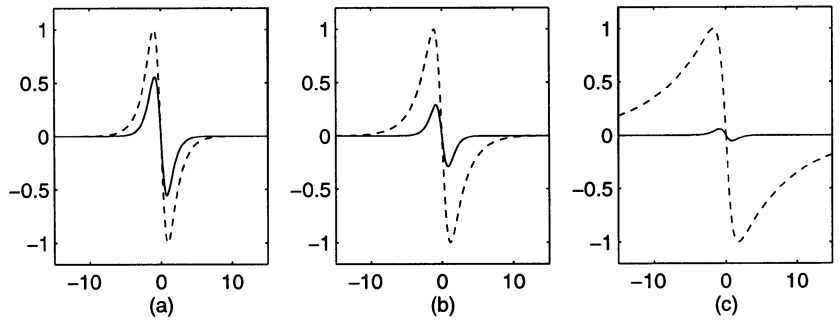


Figure 5. The discrete eigenfunctions $\psi_{\beta 0}$ for $\beta$ equal to (a) 0.05, (b) 0.2, and (c) $\frac{2}{3}$. The solid curves are $\psi_{\beta 0}[1]$ and the dashed ones are $\psi_{\beta 0}[2]$.

$L_\beta$ as $\beta$ moves from 0 to 1 leaves little doubt that they are indeed complete. As a result, any initial condition $V(x, 0)$ can be decomposed into these states as

$$V(x,0) = \int \{c^{(1)}\psi_\beta^{(1)}(x,\lambda) + c^{(2)}\psi_\beta^{(2)}(x,\lambda)\}d\lambda + c_{\beta e}\psi_{\beta e}(x) + d_{\beta e}\phi_{\beta e}(x) + c_1\psi_{\beta 0}(x) + c_2\bar{\psi}_{\beta 0}(x), \quad (3.38)$$

where the integral is over the intervals $(-\infty \quad -1)$ and $(1 \quad \infty)$ for $\lambda$. The coefficients in (3.38) can be determined from $V(x, 0)$ by a method similar to that in [12]. In particular, we find that the coefficients in front of the discrete eigenstates are

$$c_{\beta e} = \frac{\langle V(x,0),\ \phi_{\beta e}\rangle}{\langle \psi_{\beta e},\ \phi_{\beta e}\rangle}, \qquad d_{\beta e} = \frac{\langle V(x,0),\ \psi_{\beta e}\rangle}{\langle \psi_{\beta e},\ \phi_{\beta e}\rangle}, \quad (3.39a)$$

$$c_1 = \frac{\langle V(x,0),\ \psi_{\beta 0}\rangle}{\langle \psi_{\beta 0}\ \psi_{\beta 0}\rangle}, \qquad c_2 = \frac{\langle V(x,0),\ \bar{\psi}_{\beta 0}\rangle}{\langle \bar{\psi}_{\beta 0},\ \bar{\psi}_{\beta 0}\rangle} = c_1^*, \quad (3.39b)$$

where the inner product $\langle\ ,\ \rangle$ is defined in (3.19). The relation $c_2 = c_1^*$ is obtained in view of the fact that $V(x, 0) = (v(x, 0), v^*(x, 0))^{\mathrm{T}}$. The time evolution of the initial condition $V(x, 0)$ is now readily given as

$$V(x,t) = \int \{c^{(1)}\psi_\beta^{(1)}(x,\lambda) + c^{(2)}\psi_\beta^{(2)}(x,\lambda)\}e^{i\lambda t}d\lambda + c_{\beta e}\psi_{\beta e}(x) + d_{\beta e}\{\phi_{\beta e}(x) - 2it\psi_{\beta e}(x)\} + c_1\psi_{\beta 0}(x)e^{i\lambda_\beta t} + c_1^*\bar{\psi}_{\beta 0}(x)e^{-i\lambda_\beta t}. \quad (3.40)$$

It is clear from the relation (3.1) and (3.4) that the solution $V(x, t)$ causes $A$ and $B$ to evolve asymmetrically. Note that the terms $c_{\beta e}\psi_{\beta e}$ and $d_{\beta e}(\phi_{\beta e} - 2it\psi_{\beta e})$ can be absorbed into the vector soliton (3.3) and cause an opposite

phase and width shift to its $A$ and $B$ pulses respectively. More interesting are the terms $c_1\psi_{\beta 0}e^{i\lambda_\beta t} + c_2\bar{\psi}_{\beta 0}e^{-i\lambda_\beta t}$. To reveal their effects on the vector soliton (3.3), we assume that initially

$$V(x, 0) = c_1\psi_{\beta 0} + c_1^*\bar{\psi}_{\beta 0}, \tag{3.41}$$

so that its time evolution is

$$V(x, t) = c_1\psi_{\beta 0}e^{i\lambda_\beta t} + c_1^*\bar{\psi}_{\beta 0}e^{-i\lambda_\beta t}. \tag{3.42}$$

We also assume that the disturbance

$$U(x, t) = 0. \tag{3.43}$$

Then, from the relations (3.1), (3.3), and (3.4), we find that the solutions $A(x, t)$ and $B(x, t)$ are

$$A(x, t) = e^{it}(\sqrt{2/(1+\beta)}\,\mathrm{sech}\,x + \frac{1}{2}c_1\psi_{\beta 0}[1]e^{i\lambda_\beta t} + \frac{1}{2}c_1^*\psi_{\beta 0}[2]e^{-i\lambda_\beta t}), \tag{3.44a}$$

$$B(x, t) = e^{it}(\sqrt{2/(1+\beta)}\,\mathrm{sech}\,x - \frac{1}{2}c_1\psi_{\beta 0}[1]e^{i\lambda_\beta t} - \frac{1}{2}c_1^*\psi_{\beta 0}[2]e^{-i\lambda_\beta t}). \tag{3.44b}$$

If we take $\beta = 0.2$, then $\lambda_\beta \approx 0.76$ and the normalized eigenfunction $\psi_{\beta 0}$ is plotted in Figure 5b. If we further take $c_1 = 0.4$, then the amplitudes of the solutions (3.44) are plotted in Figure 6. We find that the discrete eigenmodes $\psi_{\beta 0}$ and $\bar{\psi}_{\beta 0}$ cause to (3.3) a kind of internal oscillation in which the central positions of the $A$ and $B$ pulses appear to oscillate about one another and the widths simultaneously dilate and contract, both at the same frequency $\lambda_\beta$. This combined visual effect can be clearly seen in Figure 6. In the variational principle analyses by Ueda and Kath [6] and Kaup et al. [8], these position and width oscillations were treated as two processes with independent frequencies. In our analysis, these two oscillations are just the visual effects of a single internal oscillation process caused by the discrete eigenfunctions $\psi_{\beta e}$ and $\bar{\psi}_{\beta e}$, having a single frequency $\lambda_\beta$. This internal oscillation is permanent within the linearization theory. The integral in (3.40) is a collection of dispersive wave modes and is the radiation part of the $V$ solution. It can cause the $A$ pulse of the vector soliton (3.3) to dilate (or contract) and the $B$ pulse to contract (or dilate). This out-of-phase width oscillation decays at the rate $t^{-1/2}$. Interestingly, using the variational principle method and excluding radiation, Kaup et al. [8] identified similar linear eigenmodes. But it should be pointed out that such modes they identified are not really linear eigenmodes. Rather, they are radiation modes and only cause transient oscillations to the vector solution (3.3).

The asymptotic behavior of the integral in (3.40) can be analyzed as we did for the integral in (3.20). The dispersion relation of the linear modes in

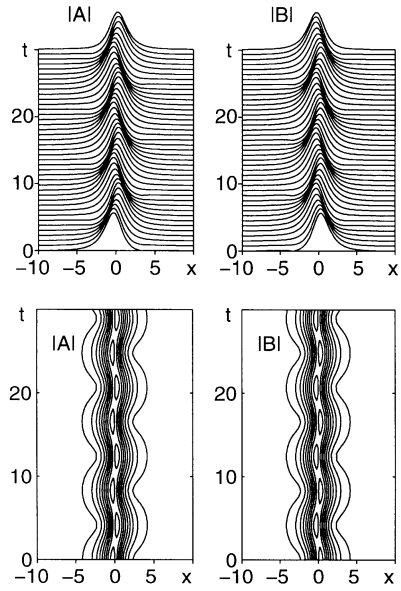


Figure 6. The solution (3.44) with $\beta = 0.2$, $c_1 = 0.4$, and $\psi_{\beta 0}$ as plotted in Figure 5b. The upper two graphs are the amplitude plots, and the lower two are the contour plots. Contours are evenly spaced at 0.1:0.15:1.3 for both $|A|$ and $|B|$.

the integral in (3.40) is again $\lambda = \pm(k^2 + 1)$, where $k$ is the wavenumber of the linear mode in the far field. When time is large, the integral for small and moderate $x$ is dominated by the low-wavenumber modes with $k \approx 0$ and $\lambda \approx \pm 1$ and decays at the rate $t^{-1/2}$. When $\beta = 0$, the modes with $k = 0$ and $\lambda = 1$ and $-1$ are

$$\psi(x, 0) = \begin{pmatrix} -\operatorname{sech}^2 x \\ \tanh^2 x \end{pmatrix}, \qquad \bar{\psi}(x, 0) = \sigma_1 \psi(x, 0), \tag{3.45}$$

which are symmetric in $x$. This indicates that, when time is large, the integral in (3.40) asymptotically becomes a symmetric low shelf at the tails of the vector soliton. When $\beta = 1$, the modes with $k = 0$ and $\lambda = 1$ and $-1$ become

$$\psi_1^{(1)}(x, 1) = \begin{pmatrix} 0 \\ 1 \end{pmatrix} \tanh x, \qquad \psi_1^{(1)}(x, -1) = \sigma_1 \psi_1^{(1)}(x, 1), \tag{3.46}$$

which are antisymmetric in $x$. In this case, when time is large, the integral in (3.40) becomes an antisymmetric low shelf at the tails of the vector soliton. When $0 < \beta < 1$, if $\beta$ is close to 0, the integral in (3.40) will asymptotically become a mainly symmetric shelf; if $\beta$ is close to 1, it will become a mainly antisymmetric shelf. This low shelf contributes to the numerically observed radiation shelf too [6].

Finally, when $\beta > 1$, the discrete eigenstate $\psi_{\beta e}$ (with $\lambda = 0$) and its generalized eigenstate $\phi_{\beta e}$ still exist, but the other two discrete eigenstates $\psi_{\beta 0}$ and $\bar{\psi}_{\beta 0}$ disappear. As a result, the permanent internal oscillations are no longer present. The other aspects of the solution evolution is similar to those with $0 < \beta < 1$.

3.1.3. *An example.* For any disturbed state of the vector soliton (3.3), the time evolution of the solution can be determined by the methods described above in view of the relations (3.1) and (3.4). As an example, we now determine the asymptotic state of the solution if initially the $A$ and $B$ pulses of the vector soliton (3.3) are slightly separated in space, i.e.,

$$A(x, 0) = \sqrt{2/(1+\beta)}\,\mathrm{sech}(x + x_0), \tag{3.47a}$$

$$B(x, 0) = \sqrt{2/(1+\beta)}\,\mathrm{sech}(x - x_0), \tag{3.47b}$$

where $x_0$ is small. In this case,

$$\tilde{A}(x, 0) = \sqrt{2/(1+\beta)}\{\mathrm{sech}(x + x_0) - \mathrm{sech}\, x\}, \tag{3.48a}$$

$$\tilde{B}(x, 0) = \sqrt{2/(1+\beta)}\{\mathrm{sech}(x - x_0) - \mathrm{sech}\, x\}, \tag{3.48b}$$

and

$$u(x, 0) = \sqrt{2/(1+\beta)}\{\mathrm{sech}(x + x_0) + \mathrm{sech}(x - x_0) - 2\,\mathrm{sech}\, x\}, \tag{3.49a}$$

$$v(x, 0) = \sqrt{2/(1+\beta)}\{\mathrm{sech}(x + x_0) - \mathrm{sech}(x - x_0)\}. \tag{3.49b}$$

First, we determine the asymptotic state of $u(x, t)$. From (3.20) we get

$$\begin{aligned} U(x, t) \longrightarrow\ & c_e\psi_e(x) + c_0\psi_0(x) + d_e\{\phi_e(x) - 2it\psi_e(x)\} \\ & + d_0\{\phi_0(x) - 2it\psi_0(x)\}, \qquad t \to \infty, \end{aligned} \tag{3.50}$$

where $c_e$, $c_0$, $d_e$, and $d_0$ are found from (3.18) to be

$$c_e = c_0 = d_0 = 0, \qquad d_e = -\int_{-\infty}^{\infty} u(x, 0)\,\mathrm{sech}\, x dx. \tag{3.51}$$

It follows that

$$u(x, t) \longrightarrow d_e\{\mathrm{sech}\, x(x \tanh x - 1) - 2it\,\mathrm{sech}\, x\}, \qquad t \to \infty. \tag{3.52}$$

Next, we determine the asymptotic state of $v(x, t)$. From (3.40) we get

$$\begin{aligned} v(x, t) \longrightarrow\ & c_{\beta e}\psi_{\beta e}(x) + d_{\beta e}(\phi_{\beta e}(x) - 2it\psi_{\beta e}) \\ & + c_1\psi_{\beta 0}e^{i\lambda_\beta t} + c_1^*\bar{\psi}_{\beta 0}e^{-i\lambda_\beta t}, \qquad t \to \infty. \end{aligned} \tag{3.53}$$

If we denote $\psi_{\beta 0} = (h_1(x,\beta), h_2(x,\beta))^{\mathrm{T}}$, then the coefficients are found from (3.39) to be

$$c_{\beta e} = d_{\beta e} = 0, \qquad c_1 = \frac{\int_{-\infty}^{\infty} v(x,0)(h_1 - h_2)dx}{\int_{-\infty}^{\infty}(h_1^2 - h_2^2)dx}. \tag{3.54}$$

Therefore,

$$v(x,t) \longrightarrow c_1\{h_1(x,\beta)e^{i\lambda_\beta t} + h_2(x,\beta)e^{-i\lambda_\beta t}\}, \qquad t \to \infty. \tag{3.55}$$

The functions $h_1$ and $h_2$, as well as $\lambda_\beta$, can be determined numerically from Equation (3.26).

The asymptotic states of $\tilde{A}$ and $\tilde{B}$ can now be obtained from (3.4), (3.52), and (3.55). So when time is large, we obtain from (3.1) and (3.3) that

$$\begin{aligned} A(x,t) \longrightarrow e^{it}\{&\sqrt{2/(1+\beta)}\,\operatorname{sech} x + \frac{1}{2}d_e[\operatorname{sech} x(x\tanh x - 1) - 2it\operatorname{sech} x] \\ &+ \frac{1}{2}c_1(h_1 e^{i\lambda_\beta t} + h_2 e^{-i\lambda_\beta t})\}, \qquad t \to \infty, \end{aligned} \tag{3.56a}$$

$$\begin{aligned} B(x,t) \longrightarrow e^{it}\{&\sqrt{2/(1+\beta)}\,\operatorname{sech} x + \frac{1}{2}d_e[\operatorname{sech} x(x\tanh x - 1) - 2it\operatorname{sech} x] \\ &- \frac{1}{2}c_1(h_1 e^{i\lambda_\beta t} + h_2 e^{-i\lambda_\beta t})\}, \qquad t \to \infty. \end{aligned} \tag{3.56b}$$

The $d_e$ terms can be absorbed into the vector soliton and cause a width shift to it. This can be easily done and we get

$$\begin{aligned} A(x,t) \longrightarrow &\sqrt{2/(1+\beta)}\, r\operatorname{sech} rx e^{ir^2 t} \\ &+ \frac{1}{2}c_1(h_1 e^{i(1+\lambda_\beta)t} + h_2 e^{i(1-\lambda_\beta)t}), \end{aligned} \tag{3.57a}$$

$$\begin{aligned} B(x,t) \longrightarrow &\sqrt{2/(1+\beta)}\, r\operatorname{sech} rx e^{ir^2 t} \\ &- \frac{1}{2}c_1(h_1 e^{i(1+\lambda_\beta)t} + h_2 e^{i(1-\lambda_\beta)t}), \end{aligned} \tag{3.57b}$$

where $r = 1 - \sqrt{(1+\beta)/8}\, d_e$. For the linearization theory to be valid, the initial disturbances $\tilde{A}(x,0)$ and $\tilde{B}(x,0)$ in (3.48) need to be small. This requires $x_0$ to be small. Under this condition, the formulas for $d_e$, $c_1$, and $r$ can be simplified. We can easily show that

$$d_e \approx \sqrt{\frac{2}{1+\beta}}\frac{x_0^2}{3}, \qquad r \approx 1 - \frac{x_0^2}{6}, \tag{3.58a}$$

$$c_1 \approx -\sqrt{\frac{8}{1+\beta}}\,\frac{\int_{-\infty}^{\infty}\operatorname{sech} x\tanh x(h_1 - h_2)dx}{\int_{-\infty}^{\infty}(h_1^2 - h_2^2)dx}\, x_0. \tag{3.58b}$$

If we take $\beta = 0.2$, then $\lambda_\beta \approx 0.76$, and the normalized eigenfunction $\psi_{\beta 0} = (h_1 \;\; h_2)^{\mathrm{T}}$ is as shown in Figure 5b. We then find numerically that

$$c_1 \approx 0.78 x_0. \tag{3.59}$$

With $r$ and $c_1$ approximated by (3.58a) and (3.59), the asymptotic state (3.57) with $x_0 = 0.5$ is plotted in Figure 7. This figure reveals that the asymptotic state (3.57) describes a permanent internal oscillation in which the central positions of the $A$ and $B$ pulses oscillate about each other while the widths of them dilate and contract simultaneously. Note that in this state, the amplitude functions $|A|$ and $|B|$ have two independent frequencies $\lambda_\beta$ and $r^2 - 1$. $\lambda_\beta$ is the frequency at which the central positions and the widths of the pulses oscillate. It is independent of the initial separation $x_0$. $r^2 - 1$ is the frequency at which the widths of the pulses are slowly modulated. It is dependent of $x_0$. Due to the presence of these two frequencies, the evolution of the amplitudes $|A|$ and $|B|$ is in general quasi-periodic rather than periodic. When compared to the numerical results in Figure 3, we find the asymptotic solution (3.57) correctly captures all the important features in the internal oscillations of (3.3), both qualitatively and quantitatively.

3.1.4. *The nature of the radiation shelf.* The low-wavenumber radiation shelf at the tails of the interacting pulses has been reported by Ueda and Kath [6] in their numerical results. This shelf is reproduced here in Figure 8 by numerically computing Equations (1.1) with $\beta = \frac{2}{3}$ and the initial condition as

$$A(x, 0) = \sqrt{2/(1+\beta)}\,\mathrm{sech}(x + 0.5), \tag{3.60a}$$

$$B(x, 0) = \sqrt{2/(1+\beta)}\,\mathrm{sech}(x - 0.5). \tag{3.60b}$$

The contour plots of these solutions for a longer time interval are graphed in Figure 9. We can observe from these contour plots that the inner side of

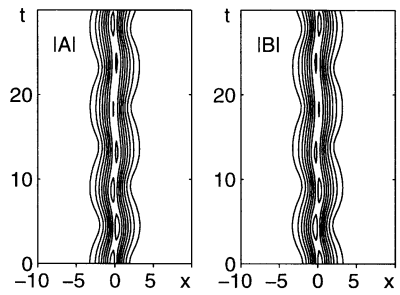


Figure 7. The contour plots of the asymptotic state (3.57) with $\beta = 0.2$ and $x_0 = 0.5$. Contours are evenly spaced at 0.2:0.15:1.25 for both $|A|$ and $|B|$.

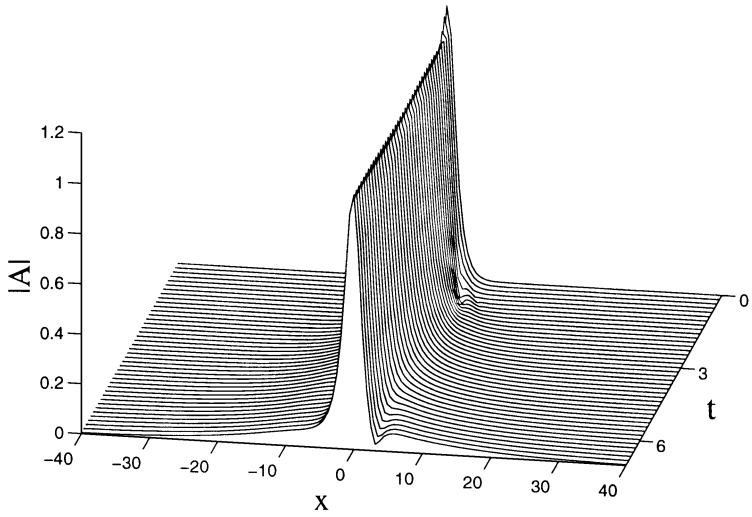


Figure 8. The radiation shelf developed in the numerical solution of Equations (1.1). The initial condition is given by (3.60) and $\beta = \frac{2}{3}$. Only $|A|$ is graphed. $|B|$ is similar.

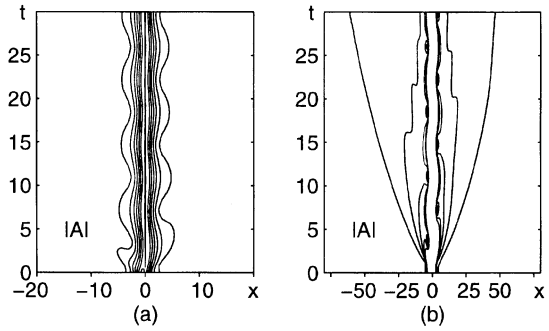


Figure 9. The contour plots of the solution $|A|$ in Figure 8 for a longer time. Contours are evenly spaced: (a) 0.1:0.15:1; (b) 0.02:0.02:0.1.

the shelf remains close to the pulses and oscillates with them for a very long time, while the outer side of it slowly propagates outward and stretches out. These solution behaviors can be readily explained now by the results from the previous linearization analysis.

The previous linearization results tell us that three factors can contribute to the radiation shelf: the low-wavenumber radiation modes in the integral of (3.20), those similar modes in the integral of (3.40), and the discrete eigenmodes $\psi_{\beta 0}$ and $\bar{\psi}_{\beta 0}$ $(= \sigma_1 \psi_{\beta 0})$ of the operator $L_\beta$. Note that when $\beta$ is smaller than but is close to 1, $\psi_{\beta 0}$ is quite flat (see Figure 5c). Therefore, the eigenmodes $\psi_{\beta 0}$ and $\bar{\psi}_{\beta 0}$ will bring a low oscillating shelf to the vector soli-

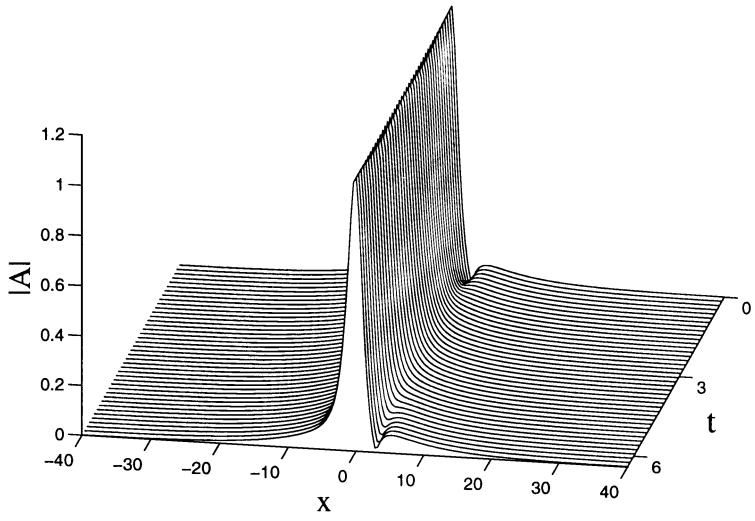


Figure 10. The solution (3.44) with $\beta = \frac{2}{3}$, $c_1 = 0.25$ and $\psi_{\beta 0}$ as plotted in Figure 5c. Low-radiation shelf can be observed. Only $|A|$ is plotted. $|B|$ is similar.

ton (3.3). To demonstrate this, we plot in Figure 10 the solution (3.44) with $\beta = \frac{2}{3}$ and $c_1 = 0.25$. The eigenfunction $\psi_{\beta 0}$ is as shown in Figure 5c. As expected, we observe a low shelf similar to that in Figure 8. In the contour plots of solution (3.44) shown in Figure 11, we can see that for all time, this shelf remains close to the pulses and oscillates with them at frequency $\lambda_\beta$, which is approximately equal to 0.982 when $\beta$ is $\frac{2}{3}$ (see Figure 4). It is now clear that the oscillating inner shelf in Figure 9 is caused by the eigenmodes $\psi_{\beta 0}$ and $\bar{\psi}_{\beta 0}$ and is only a special case of the linearly permanent internal oscillations discussed before. This is why this inner shelf can stay close to and oscillate with the pulses for a long time. The slowly propagating outer shelf observed in Figure 9 is due to the low-wavenumber radiation modes in the integrals of (3.20) and (3.40). These modes have small group velocities and propagate slowly. Due to dispersion, they decay at the rate $t^{-1/2}$. As time gets large, these low-wavenumber radiation modes will be seen at the outer side of the shelf. At the inner side of the shelf, the radiation modes will be negligible and the eigenmodes $\psi_{\beta 0}$ and $\bar{\psi}_{\beta 0}$ will be dominating and cause long-lasting internal oscillations to the pulses. Finally, we comment that when $\beta$ is not close to 1, either the discrete eigenmodes $\psi_{\beta 0}$ and $\bar{\psi}_{\beta 0}$ exist but are not flat (for $\beta < 1$, see Figure 5), or $\psi_{\beta 0}$ and $\bar{\psi}_{\beta 0}$ do not exist at all (when $\beta > 1$). In both cases, the radiation shelf will be contributed solely by the low-wavenumber radiation modes in the integrals of (3.20) and (3.40). Therefore, this shelf will disperse away and decay and will be less visible at the tails of the pulses.

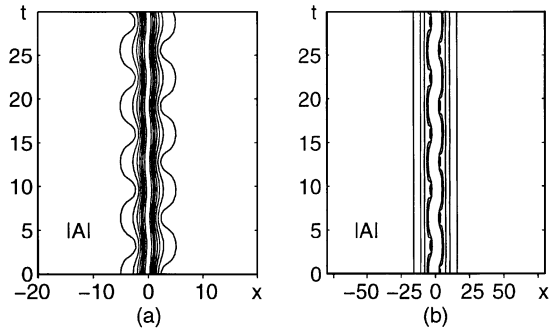


Figure 11. The contour plots of the solution $|A|$ in Figure 10 for a longer time. Contours are evenly spaced: (a) 0.1:0.15:1; (b) 0.02:0.02:0.1.

### *3.2. Linearization analysis for general single-hump vector solitons*

For general single-hump vector solitons (2.1) of arbitrary polarization, the disturbances $\tilde{A}$ and $\tilde{B}$ are governed by Equations (3.2). We denote $\mathscr{R} \equiv (\tilde{A}, \tilde{A}^*, \tilde{B}, \tilde{B}^*)^{\mathrm{T}}$. Then the linear system for $\mathscr{R}$ can be readily obtained from (3.2). It is

$$i\mathscr{R}_t + \mathscr{L}\mathscr{R} = 0, \tag{3.61}$$

where the operator $\mathscr{L}$ is

$$\mathscr{L} = \begin{pmatrix} (\partial_{xx} - 1 + 2r_1^2 + \beta r_2^2)\sigma_3 + ir_1^2\sigma_2 & \beta r_1 r_2(\sigma_3 + i\sigma_2) \\ \beta r_1 r_2(\sigma_3 + i\sigma_2) & (\partial_{xx} - \omega + 2r_2^2 + \beta r_1^2)\sigma_3 + ir_2^2\sigma_2 \end{pmatrix}. \tag{3.62}$$

The eigenstates of $\mathscr{R}$ are of the form

$$\mathscr{R} = e^{i\lambda t}\Psi(x), \tag{3.63}$$

where

$$\mathscr{L}\Psi = \lambda\Psi. \tag{3.64}$$

Recall that single-hump vector solitons (2.1) exist for $\omega$ in the interval $(\omega_{\mathrm{I}}, \omega_{\mathrm{II}})$, which is illustrated in Figure 2. For these single-hump solitons, the operator $\mathscr{L}$ has the following three discrete eigenmodes with $\lambda = 0$:

$$\Psi_{e1} = \begin{pmatrix} r_1 \\ -r_1 \\ r_2 \\ -r_2 \end{pmatrix}, \qquad \Psi_{e2} = \begin{pmatrix} r_1 \\ -r_1 \\ -r_2 \\ r_2 \end{pmatrix}, \qquad \Psi_0 = \begin{pmatrix} r_{1x} \\ r_{1x} \\ r_{2x} \\ r_{2x} \end{pmatrix}. \tag{3.65}$$

These states, when absorbed into the vector soliton (2.1), cause a phase, opposite phase, and position shift respectively. In the special case of solitons of equal amplitudes (3.3), they reduce to

$$\begin{pmatrix} \psi_e \\ \psi_e \end{pmatrix}, \qquad \begin{pmatrix} \psi_{\beta e} \\ -\psi_{\beta e} \end{pmatrix}, \qquad \begin{pmatrix} \psi_0 \\ \psi_0 \end{pmatrix},$$

which have been found before in the last subsection. The operator $\mathscr{L}$ also has three generalized eigenstates $\Phi_{e1}$, $\Phi_{e2}$, and $\Phi_0$, where

$$\mathscr{L}\Phi_{e1} = -2\Psi_{e1}, \qquad \mathscr{L}\Phi_{e2} = -2\Psi_{e2}, \qquad \mathscr{L}\Phi_0 = -2\Psi_0. \tag{3.66}$$

These states are the counterparts of the modes $\phi_e$, $\phi_{\beta e}$, and $\phi_0$ in the solitons of equal amplitudes. They cause a width, opposite width, and velocity shift to the vector soliton (2.1). These states can be determined numerically.

When $0 < \beta < 1$, the operator $\mathscr{L}$ has two more discrete eigenmodes, $\Psi_{\mathscr{L}0}$ with a nonzero eigenvalue $\lambda_{\mathscr{L}}(> 0)$, and $\bar{\Psi}_{\mathscr{L}0} = \sigma_4 \Psi_{\mathscr{L}0}$ with $-\lambda_{\mathscr{L}}$, where

$$\sigma_4 = \begin{pmatrix} \sigma_1 & 0 \\ 0 & \sigma_1 \end{pmatrix}.$$

These modes are the counterparts of $\psi_{\beta 0}$ and $\bar{\psi}_{\beta 0}$ in the last subsection and can be determined numerically. For instance, if $\beta = 0.2$ and $\omega = 0.5$, then the single-hump vector soliton (2.1) is plotted in Figure 12, and $\Psi_{\mathscr{L}0}$ is plotted in Figure 13 with $\lambda_{\mathscr{L}} \approx 0.486$. This eigenfunction has been normalized so that the maximum of the four functions in $\Psi_{\mathscr{L}0}$ is equal to 1. The dependence of $\lambda_{\mathscr{L}}$ on $\omega$ that results if we freeze $\beta = 0.2$ and allow $\omega$ to change from $\omega_{\mathrm{I}}$ to $\omega_{\mathrm{II}}$, i.e., approximately from 0.094 to 10.66, is plotted in Figure 14. As $\omega$ moves down to its lower boundary value 0.094, $\lambda_{\mathscr{L}}$ approaches $\omega$, and $\Psi_{\mathscr{L}0}[3]$ and $\Psi_{\mathscr{L}0}[4]$ get flat for large $x$. On the other hand, when $\omega$ moves up to its upper boundary value 10.66, $\lambda_{\mathscr{L}}$ approaches 1, and $\Psi_{\mathscr{L}0}[1]$ and $\Psi_{\mathscr{L}0}[2]$ become flat for large $x$. If we freeze $\beta$ to be other values between 0 and 1 and change $\omega$ from $\omega_{\mathrm{I}}$ to $\omega_{\mathrm{II}}$, then the $(\lambda_{\mathscr{L}}, \quad \omega)$ curve and the shape change in $\Psi_{\mathscr{L}0}$ are similar to that with $\beta = 0.2$.

The eigenmodes $\Psi_{\mathscr{L}0}$ and $\bar{\Psi}_{\mathscr{L}0}$ cause a similar permanent internal oscillation to the vector soliton (2.1) as the modes $\psi_{\beta 0}$ and $\bar{\psi}_{\beta 0}$ do to the vector soliton of equal amplitudes (3.3). The difference is that the degree of oscillations is now different for the $A$ and $B$ pulses. Let us take $\beta = 0.2$ and $\omega = 0.5$ as an example. The vector soliton for this case has been plotted in Figure 12. The discrete eigenfunction $\Psi_{\mathscr{L}0}$ has been plotted in Figure 13 with $\lambda_{\mathscr{L}} \approx 0.486$. Assume that the initial disturbance is

$$\mathscr{R}(x, 0) = c_1 \Psi_{\mathscr{L}0}(x) + c_2 \bar{\Psi}_{\mathscr{L}0}(x), \tag{3.67}$$

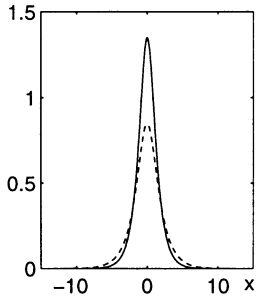


Figure 12. The vector soliton (2.1) for $\beta = 0.2$ and $\omega = 0.5$. Solid curve, $r_1(x)$; dashed curve, $r_2(x)$.

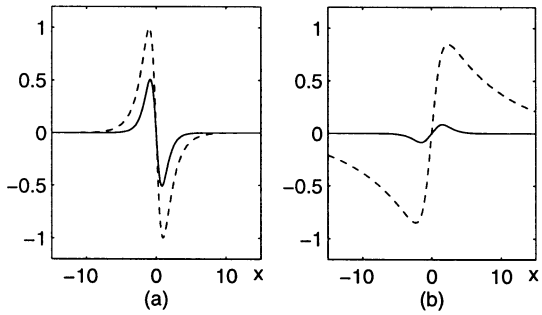


Figure 13. The discrete eigenfunction $\Psi_{\mathscr{L}0}$ for the vector soliton (2.1) with $\beta = 0.2$ and $\omega = 0.5$. (a) solid, $\Psi_{\mathscr{L}0}[1]$; dashed, $\Psi_{\mathscr{L}0}[2]$; (b) solid, $\Psi_{\mathscr{L}0}[3]$; dashed, $\Psi_{\mathscr{L}0}[4]$.

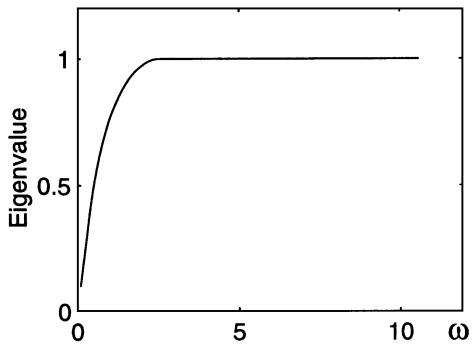


Figure 14. Dependence of the operator $\mathscr{L}$'s discrete eigenvalue $\lambda_{\mathscr{L}}$ on $\omega$ when $\beta$ is frozen to be 0.2.

where $c_1$ and $c_2$ are small complex constants. It can be shown that the relation $c_1 = c_2^*$ needs to be satisfied to ensure consistency. Then the later time evolution for $\mathscr{R}$ is

$$\mathscr{R}(x, t) = c_1 \Psi_{\mathscr{L}0}(x) e^{i\lambda_{\mathscr{L}} t} + c_2 \bar{\Psi}_{\mathscr{L}0}(x) e^{-i\lambda_{\mathscr{L}} t}. \tag{3.68}$$

It follows that the solutions $A$ and $B$ are

$$A(x, t) = e^{it}\{r_1(x) + c_1 \Psi_{\mathscr{L}0}[1] e^{i\lambda_{\mathscr{L}} t} + c_2 \Psi_{\mathscr{L}0}[2] e^{-i\lambda_{\mathscr{L}} t}\}, \tag{3.69a}$$

$$B(x, t) = e^{it}\{r_2(x) + c_1 \Psi_{\mathscr{L}0}[3] e^{i\lambda_{\mathscr{L}} t} + c_2 \Psi_{\mathscr{L}0}[4] e^{-i\lambda_{\mathscr{L}} t}\}. \tag{3.69b}$$

If we further take $c_1 = c_2 = 0.2$, then the amplitudes of $A$ and $B$ are plotted in Figure 15. One can observe that these oscillations are similar to those in Figure 6, except that here the oscillation in $|B|$ is stronger than it is in $|A|$. Within the linearization theory, these oscillations are permanent with frequency $\lambda_{\mathscr{L}}$.

When $\beta \geq 1$, the discrete eigenstates $\Psi_{\mathscr{L}0}$ and $\bar{\Psi}_{\mathscr{L}0}$ disappear and no permanent internal oscillations exist any more. The continuous spectrum of the operator $\mathscr{L}$ is $|\lambda| > \min(1, \omega)$. These continuous eigenmodes can be readily determined numerically. These modes, together with the above discrete eigenmodes and their generalized eigenmodes, also form a complete set. Any

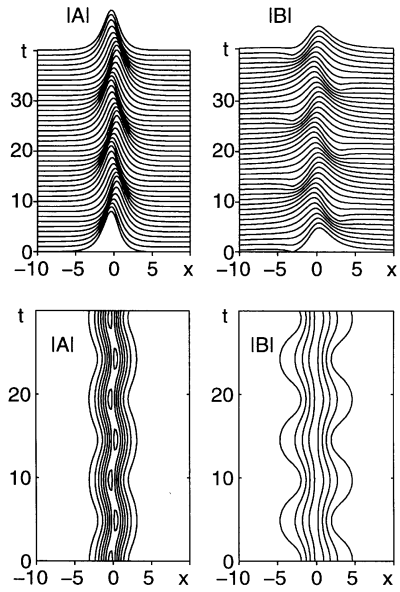


Figure 15. The solution (3.69) with $\beta = 0.2$, $\omega = 0.5$, $c_1 = c_2 = 0.2$, and $\Psi_{\mathscr{L}0}$ as shown in Figure 13. The top two graphs are the amplitude plots, and the bottom two are the contour plots. Contours are evenly spaced: 0.2:0.2:1.4 for $|A|$ and 0.2:0.2:0.8 for $|B|$.

initial disturbance $\tilde{A}(x,0)$ and $\tilde{B}(x,0)$ can be decomposed into these eigenstates. Therefore, its time evolution can be easily determined. This analysis is similar to what we did in the last section and is not reproduced here.

### *3.3. Linearization analysis for degenerate vector solitons*

The degenerate vector solitons, in which one of the $A$ and $B$ components vanishes, are different from the single-hump vector solitons (2.1) described in Section 2. A separate linearization analysis is needed to study their internal oscillations.

Without loss of generality, we assume that the degenerate vector soliton is

$$A = \sqrt{2}\,\mathrm{sech}\, x e^{it}, \qquad B = 0. \tag{3.70}$$

When it is disturbed, then

$$A = e^{it}(\sqrt{2}\,\mathrm{sech}\, x + \tilde{A}), \qquad B = \tilde{B}, \tag{3.71}$$

where $\tilde{A}$ and $\tilde{B}$ are small disturbances. When (3.71) is substituted into (1.1) and higher-order terms neglected, then the linearized equations for $\tilde{A}$ and $\tilde{B}$ are

$$i\tilde{A}_t + \tilde{A}_{xx} - \tilde{A} + 4\,\mathrm{sech}^2 x\tilde{A} + 2\,\mathrm{sech}^2 x\tilde{A}^* = 0, \tag{3.72}$$

$$i\tilde{B} + \tilde{B}_{xx} + 2\beta\,\mathrm{sech}^2 x\tilde{B} = 0. \tag{3.73}$$

Equation (3.72) is the same as (3.5) whose solution has been given in Section 3.1. An initial disturbance in $\tilde{A}$ may cause phase, position, width, and velocity shifts to the $A$ soliton, but there is no permanent internal oscillations involved. Equation (3.73) is the time-dependent linear Schrödinger equation. Its eigenstates are

$$\tilde{B} = e^{i\lambda t} b(x), \tag{3.74}$$

where

$$M_\beta b = \lambda b, \tag{3.75}$$

and

$$M_\beta = \partial_{xx} + 2\beta\,\mathrm{sech}^2 x \tag{3.76}$$

is the Schrödinger operator and is Hermitian. It is well known in quantum mechanics that Equation (3.75) can be solved exactly [13] and the eigensolutions $(b(x), \lambda)$ can be analytically determined. When $0 < \beta \leq 1$, the operator $M_\beta$ has a single discrete eigenstate

$$b_1(x) = \mathrm{sech}^s x, \qquad \lambda_1 = \frac{1}{4}(\sqrt{1+8\beta} - 1)^2, \tag{3.77}$$

where $s = (\sqrt{1+8\beta} - 1)/2$. This state is reminiscent of the daughter wave state of a vector soliton (2.1). When $1 < \beta \leq 3$, beside $(b_1(x), \lambda_1)$, $M_\beta$ has one more discrete eigenstate

$$b_2(x) = \operatorname{sech}^s x \sinh x, \qquad \lambda_2 = \frac{1}{4}(\sqrt{1+8\beta} - 3)^2. \tag{3.78}$$

When $\beta > 3$, even more discrete eigenstates will appear.

The continuous spectrum of $M_\beta$ is $\lambda \leq 0$ when $\beta = n(n+1)/2, (n = 1, 2, \ldots)$, and $\lambda < 0$ for other positive values of $\beta$. The continuous eigenfunctions can be expressed in terms of the hypergeometric functions. They, together with the above discrete eigenfunctions, form a complete set since $M_\beta$ is Hermitian.

An initial disturbance in $\tilde{B}$ can be decomposed into the eigenstates of $M_\beta$. The collection of the continuous eigenmodes corresponds to radiation and decays at the rate $t^{-1/2}$. The discrete eigenmodes will persist for all time. When $0 < \beta \leq 1$, there is only one such mode. Therefore, when time is large, $\tilde{B}$ will asymptotically approach this eigenstate in which no amplitude oscillations are present. But when $\beta > 1$, two or more discrete eigenmodes exist. Hence, $\tilde{B}$ will asymptotically approach a state which is a linear superposition of these discrete eigenmodes. In this state, the amplitude oscillates permanently with time. For demonstration purposes, let us suppose that initially there is no $\tilde{A}$ disturbance, and $\tilde{B}$ consists of only the two lowest discrete eigenmodes, i.e.,

$$\tilde{A}(x, 0) = 0, \qquad \tilde{B}(x, 0) = c_1 b_1(x) + c_2 b_2(x), \tag{3.79}$$

where $c_1$ and $c_2$ are two arbitrary small complex constants. Then, the time evolution for $A$ and $B$ is

$$A(x, t) = \sqrt{2} \operatorname{sech} x e^{it}, \tag{3.80a}$$

$$B(x, t) = c_1 b_1(x) e^{i\lambda_1 t} + c_2 b_2(x) e^{i\lambda_2 t}. \tag{3.80b}$$

If we take $\beta = 2$ and $c_1 = c_2 = 0.3$, then their amplitudes are plotted in Figure 16. In the solution (3.80), $|A|$ does not change with time, but $|B|$ oscillates back and forth with frequency $\lambda_1 - \lambda_2 = \sqrt{1+8\beta} - 2$. This oscillation in $|B|$ is also permanent within the linearization theory.

## 4. Higher-order effects

The linearization analysis in the last section shows that small disturbances may cause permanent internal oscillations as well as phase, position, width,

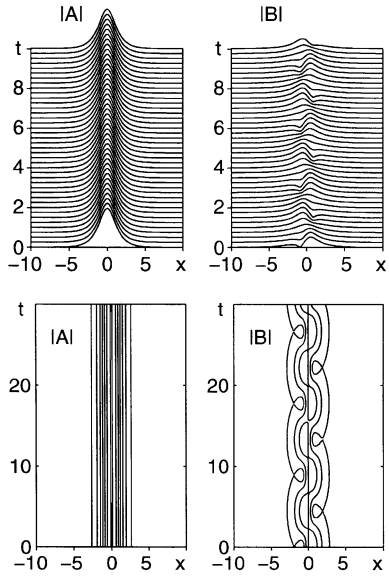


Figure 16. The solution (3.80) with $\beta = 2$ and $c_1 = c_2 = 0.3$. The top two graphs are the amplitude plots, and the bottom two are the contour plots. Contours are evenly spaced: 0.2:0.2:1.4 for $|A|$ and 0.1:0.1:0.3 for $|B|$.

and velocity shifts to a vector soliton. When higher-order effects are taken into consideration, the phase, position, width, and velocity shifts will just be slightly modified. But how the linearly permanent internal oscillations are affected is still not clear. This question is now studied in this section.

The linearly permanent internal oscillations arise for single-hump vector solitons when $0 < \beta < 1$ and for degenerate vector solitons when $\beta > 1$. For simplicity while without losing generality, we just study the higher-order effects on these oscillations for vector solitons of equal amplitudes (3.3) and for the degenerate vector solitons (3.70). The analysis for arbitrary single-hump vector solitons is similar.

### *4.1. Analysis for degenerate vector solitons*

When the degenerate vector soliton (3.70) is perturbed, the solutions $A$ and $B$ can be expanded in the perturbation series

$$A(x, t) = e^{it}\{\sqrt{2}\,\mathrm{sech}\, x + \epsilon A_1 + \epsilon^2 A_2 + \ldots\}, \tag{4.1a}$$

$$B(x, t) = \epsilon B_1 + \epsilon^2 B_2 + \ldots, \tag{4.1b}$$

where $\epsilon$ is a small parameter that measures the size of the disturbance. At

order $\epsilon$, the equations for $A_1$ and $B_1$ are

$$iA_{1t} + A_{1xx} - A_1 + 4\,\mathrm{sech}^2\, xA_1 + 2\,\mathrm{sech}^2\, xA_1^* = 0, \tag{4.2}$$

$$iB_{1t} + B_{1xx} + 2\beta\,\mathrm{sech}^2\, xB_1 = 0. \tag{4.3}$$

These equations are the same as (3.72) and (3.73). Actually, if order $\epsilon^2$ and higher terms in (4.1) are neglected, this analysis will become the linearization analysis as in Section 3, and the solutions for $A_1$ and $B_1$ have been determined there. The linearly permanent internal oscillations are present in the $B_1$ solution when $\beta > 1$. They are caused by two or more discrete eigenmodes of the operator $M_\beta$. Since our objective is to study the higher-order effects on these permanent oscillations, for simplicity, we take

$$A_1(x, t) = 0, \qquad B_1(x, t) = c_1 b_1(x) e^{i\lambda_1 t} + c_2 b_2(x) e^{i\lambda_2 t}, \tag{4.4}$$

where $b_i$ and $\lambda_i$ $(i = 1, 2)$ are given by (3.77) and (3.78), and $c_i$ $(i = 1, 2)$ are arbitrary complex constants. At order $\epsilon_2$, $A_2$ is governed by the equation

$$iA_{2t} + A_{2xx} - A_2 + 4\,\mathrm{sech}^2\, xA_2 + 2\,\mathrm{sech}^2\, xA_2^* = \eta, \tag{4.5}$$

where

$$\eta = -\sqrt{2}\beta\,\mathrm{sech}\, x\{c_1 c_1^* b_1^2 + c_2 c_2^* b_2^2 + (c_1 c_2^* e^{i(\lambda_1-\lambda_2)t} + c_1^* c_2 e^{-i(\lambda_1-\lambda_2)t}) b_1 b_2\}. \tag{4.6}$$

To find its solution, we work with the variables $A_2$ and $A_2^*$. Let us denote $W = (A_2, A_2^*)^{\mathrm{T}}$. Then $W$ satisfies the equation

$$iW_t + LW = \eta \begin{pmatrix} 1 \\ -1 \end{pmatrix}, \tag{4.7}$$

where the operator $L$ is given by Equation (3.8). Recall that the homogeneous equation of (4.7) has been solved exactly in Section 3. Therefore, once we can find an inhomogeneous solution $W_p$ to (4.7), then (4.7) will be solved. Since Equation (4.7) is linear, $W_p$ can be written as

$$W_p(x, t) = -\sqrt{2}\beta \Bigg\{ (c_1 c_1^* w_1(x) + c_2 c_2^* w_2(x)) \begin{pmatrix} 1 \\ 1 \end{pmatrix} + c_1 c_2^* w_3(x) e^{i(\lambda_1-\lambda_2)t} + c_1^* c_2 w_4(x) e^{-i(\lambda_1-\lambda_2)t} \Bigg\}, \tag{4.8}$$

where the scalar functions $w_1, w_2$ and the vector functions $w_3, w_4$ are inho-

mogeneous solutions of the following equations:

$$w_{1xx} - w_1 + 6\,\mathrm{sech}^2\, x w_1 = b_1^2\,\mathrm{sech}\, x, \tag{4.9}$$

$$w_{2xx} - w_2 + 6\,\mathrm{sech}^2\, x w_2 = b_2^2\,\mathrm{sech}\, x, \tag{4.10}$$

$$Lw_3 - (\lambda_1 - \lambda_2)w_3 = b_1 b_2\,\mathrm{sech}\, x \begin{pmatrix} 1 \\ -1 \end{pmatrix}, \tag{4.11}$$

$$Lw_4 + (\lambda_1 - \lambda_2)w_4 = b_1 b_2\,\mathrm{sech}\, x \begin{pmatrix} 1 \\ -1 \end{pmatrix}. \tag{4.12}$$

The homogeneous equations of (4.9) and (4.10) have a localized solution, $\mathrm{sech}\, x \tanh x$, which is orthogonal to the inhomogeneous terms $b_1^2\,\mathrm{sech}\, x$ and $b_2^2\,\mathrm{sech}\, x$, i.e.,

$$\int_{-\infty}^{\infty} b_1^2\,\mathrm{sech}^2\, x \tanh x dx = 0, \qquad \int_{-\infty}^{\infty} b_2^2\,\mathrm{sech}^2\, x \tanh x dx = 0. \tag{4.13}$$

Therefore, localized inhomogeneous solutions exist in Equations (4.9) and (4.10). These solutions can be written as

$$w_i = w_{ip} + \alpha\,\mathrm{sech}\, x \tanh x, \qquad i = 1, 2, \tag{4.14}$$

where $w_{ip}, i = 1, 2$ are inhomogeneous solutions of (4.9) and (4.10), and $\alpha$ is a real-valued constant. To make $w_{1p}$ and $w_{2p}$ unique, we can require that they are even functions of $x$. These solutions can be determined numerically if $\beta$ is given.

Next, we consider the solutions of Equations (4.11) and (4.12). For $\beta > 1$, which is the case we are considering,

$$\lambda_1 - \lambda_2 = \sqrt{1 + 8\beta} - 2 > 1. \tag{4.15}$$

So $\lambda_1 - \lambda_2$ is in the continuous spectrum of the operator $L$. As a result, the homogeneous equation of (4.11) has two linearly independent bounded solutions $\psi(x, k)$ and $\psi(x, -k)$ (note that $\psi(x, -k) = \psi^*(x, k)$), where the function $\psi(x, k)$ is given by (3.12),

$$k^2 = \lambda_1 - \lambda_2 - 1 = \sqrt{1 + 8\beta} - 3, \tag{4.16}$$

and $k > 0$. Note that $\psi(x, k)$ and $\psi(x, -k)$ have oscillating tails at infinity. For Equation (4.11), localized inhomogeneous solutions exist if and only if the compatibility condition

$$I(\beta) \equiv \int_{-\infty}^{\infty} \psi^{\mathrm{T}}(x, k)\sigma_3 b_1 b_2\,\mathrm{sech}\, x \begin{pmatrix} 1 \\ -1 \end{pmatrix} dx = 0 \tag{4.17}$$

is satisfied. But this is not the case. The magnitude of $I(\beta)$ against $\beta$ is plotted in Figure 17. We can observe that $I(\beta)$ is never equal to zero for $\beta > 1$. This indicates that Equation (4.11) has no localized inhomogeneous solutions. All its bounded solutions are not localized. Instead, they are oscillatory at infinity. Similarly, the homogeneous equation of (4.12) has two linearly independent solutions $\bar{\psi}(x, k) = \sigma_1 \psi(x, k)$ and $\bar{\psi}(x, -k) = \sigma_1 \psi^*(x, k)$. The compatibility condition for the existence of localized inhomogeneous solutions in Equation (4.12) can be shown to be the same as (4.17), which is never satisfied. Therefore, all inhomogeneous solutions of Equation (4.12) are not localized either. They also have oscillating tails at infinity.

Now we consider the initial value problem of Equation (4.5). Suppose initially that $A_2(x, 0)$ is equal to zero or is any localized function. The forcing terms in (4.5) will generate a response in the solution $A_2(x, t)$. The presence of infinity-oscillating tails in the inhomogeneous solution (4.8) reveals that $A_2$ will gradually develop and spread out such oscillating tails. These tails have frequencies $\pm(\lambda_1 - \lambda_2) = \pm(\sqrt{1 + 8\beta} - 2)$ and wavenumbers $k = \pm\sqrt{\sqrt{1 + 8\beta} - 3}$, and they travel to infinity at their group velocity $2k$. Due to this energy drain to the oscillating tails at infinity, the linearly permanent internal oscillations in (3.80) (see Figure 16) are unstable. They will become weaker and weaker until they eventually disappear. As for the solution (4.1), it will gradually lose its oscillational energy to the oscillating tails and asymptotically approach a single-hump vector soliton (2.1) of wave and daughter-wave structure. These predictions can be verified in Figures 18 and 19, where the numerical solution of Equations (1.1) is plotted with $\beta = 2$ and the initial condition as

$$A(x, 0) = \sqrt{2}\,\mathrm{sech}\, x, \qquad B(x, 0) = c_1 b_1(x) + c_2 b_2(x), \tag{4.18}$$

with $c_1 = c_2 = 0.3$. Within the linearization theory in Section 3, such initial conditions will lead to the solution (3.80) with permanent internal os-

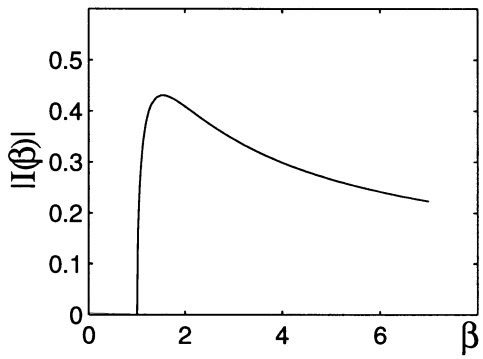


Figure 17. Dependence of the magnitude of $I(\beta)$ on $\beta$.

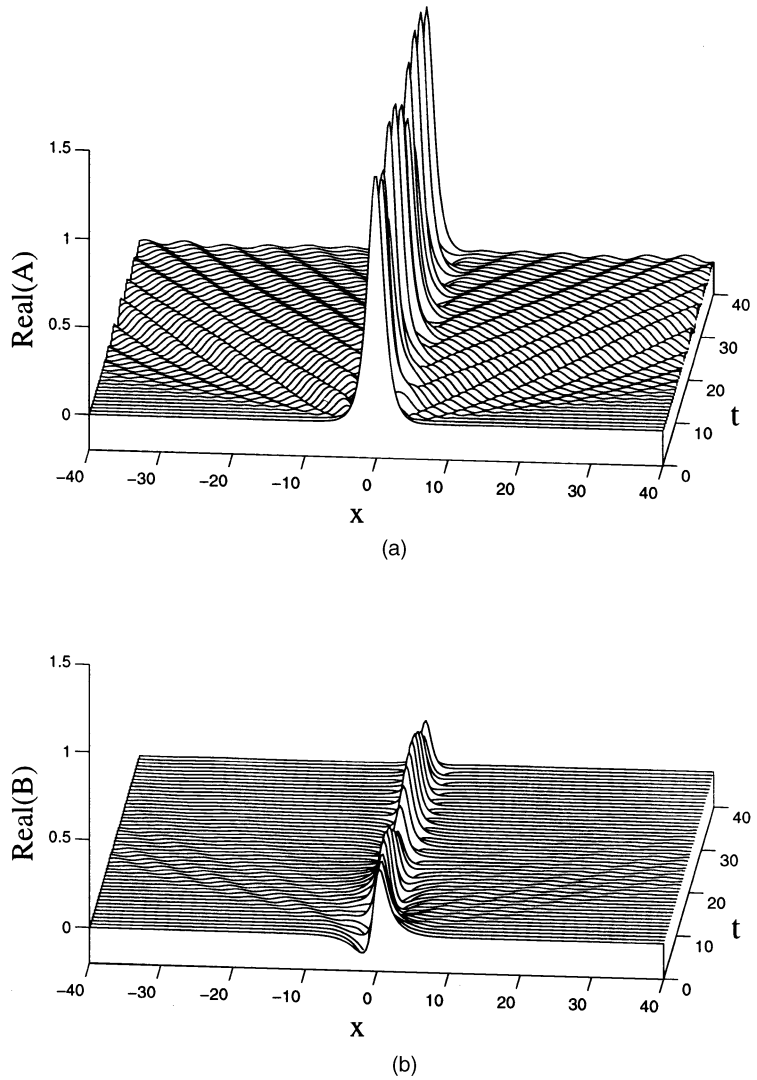


Figure 18. The numerical solution of Equations (1.1) with $\beta = 2$. The initial condition is (4.18) with $c_1 = c_2 = 0.3$. These two graphs are the Real($A$) and Real($B$) plots. The Im($A$) and Im($B$) plots are similar.

cillations (see Figure 16). But in this numerical solution where higher-order effects are automatically included, we observe that the oscillating tails are continuously emitted from the $A$ pulse, and the internal oscillation in the $B$ pulse is disappearing. The dominant wavelength of these oscillating tails in the $A$ component is approximately equal to 5.8, which is very close to the theoretically predicted value $2\pi/\sqrt{\sqrt{17}-3} \approx 5.93$. The $B$ component also

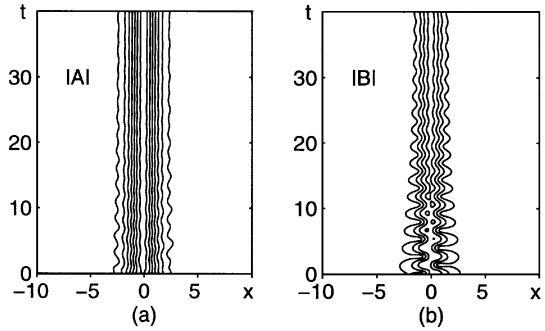


Figure 19. The contour plots of the numerical solution in Figure 18. The contours are evenly spaced: (a) $|A|$ at 0.2:0.2:1.4; (b) $|B|$ at 0.1:0.1:0.4.

develops oscillating tails. But it occurs at higher orders and is less visible. When time is large, the numerical solution approaches a single-hump vector soliton (2.1) with $(\omega_1, \omega_2) \approx (1.26, 2.73)$ and $(r_1(0), r_2(0)) \approx (1.49, 0.42)$ plus some radiation.

The energy transfer from the linearly permanent internal oscillations to the infinity-oscillating tails may also be called radiation. But this radiation takes place at second order in $\epsilon$ and is therefore very weak. As a result, these permanent internal oscillations can persist for a long time before they disappear.

### *4.2. Analysis for vector solitons of equal amplitudes*

It is helpful here to work with the two new variables

$$p = A + B, \qquad q = A - B \tag{4.19}$$

instead of $A$ and $B$. The equations for $p$ and $q$ are

$$ip_t + p_{xx} + \left(\frac{\beta+1}{4}|p|^2 + \frac{1}{2}|q|^2\right)p + \frac{1-\beta}{4}q^2p^* = 0, \tag{4.20a}$$

$$iq_t + q_{xx} + \left(\frac{\beta+1}{4}|q|^2 + \frac{1}{2}|p|^2\right)q + \frac{1-\beta}{4}p^2q^* = 0. \tag{4.20b}$$

For the vector soliton of equal amplitudes (3.3), we have

$$p = \sqrt{8/(1+\beta)}\ \operatorname{sech} x e^{it}, \qquad q = 0. \tag{4.21}$$

When it is disturbed, the solutions can be expanded in the following perturbation series:

$$p = e^{it}\left\{\sqrt{8/(1+\beta)}\ \operatorname{sech} x + \epsilon p_1 + \epsilon^2 p_2 + \cdots\right\}, \tag{4.22a}$$

$$q = e^{it}\{\epsilon q_1 + \epsilon^2 q_2 + \cdots\}, \tag{4.22b}$$

where $\epsilon$ is a small parameter measuring the size of the disturbance. The following analysis is analogous to that for the degenerate vector solitons in the previous subsection. At order $\epsilon$, the equations for $p_1$ and $q_1$ are found to be

$$ip_{1t} + p_{1xx} - p_1 + 4\,\mathrm{sech}^2\, x p_1 + 2\,\mathrm{sech}^2\, x p_1^* = 0, \tag{4.23}$$

$$iq_{1t} + q_{1xx} - q_1 + \frac{4}{1+\beta}\,\mathrm{sech}^2\, x q_1 + \frac{2(1-\beta)}{1+\beta}\,\mathrm{sech}^2\, x q_1^* = 0. \tag{4.24}$$

Note that Equations (4.23) and (3.5) are the same, and (4.24) and (3.6) are the same. If $\epsilon^2$ and higher-order terms in (4.22) are neglected, the analysis will become the linearization analysis done in Section 3, and the solutions for $p_1$ and $q_1$ are as given by (3.20) and (3.40). The linearly permanent internal oscillations of the vector soliton (3.3) are caused by $q_1$'s eigenmodes $\psi_{\beta 0}$ and $\bar{\psi}_{\beta 0}$. To examine the higher-order effects on these permanent oscillations, for simplicity we take

$$p_1 = 0, \qquad q_1 = c\; h_1(x,\beta)e^{i\lambda_\beta t} + c^* h_2(x,\beta)e^{-i\lambda_\beta t}, \tag{4.25}$$

where $\psi_{\beta 0} = (h_1, h_2)^{\mathrm{T}}$ and $c$ is an arbitrary complex constant. At order $\epsilon^2$, $p_2$ is governed by the equation

$$\begin{aligned} &ip_{2t} + p_{2xx} - p_2 + 4\,\mathrm{sech}^2\, x p_2 + 2\,\mathrm{sech}^2\, x p_2^* \\ &\quad = -\sqrt{2/(1+\beta)}\,\{cc^*\delta_0(x) + c^2\delta_1(x)e^{2i\lambda_\beta t} + c^{*2}\delta_2(x)e^{-2i\lambda_\beta t}\}, \end{aligned} \tag{4.26}$$

where

$$\delta_0 = \mathrm{sech}\, x\{h_1^2 + (1-\beta)h_1h_2 + h_2^2\}, \tag{4.27a}$$

$$\delta_1 = \mathrm{sech}\, x\left\{h_1h_2 + \frac{1}{2}(1-\beta)h_1^2\right\}, \tag{4.27b}$$

$$\delta_2 = \mathrm{sech}\, x\left\{h_1h_2 + \frac{1}{2}(1-\beta)h_2^2\right\}. \tag{4.27c}$$

We work with the variables $p_2$ and $p_2^*$ and denote $\mathscr{D} = (p_2, p_2^*)^{\mathrm{T}}$. Then $\mathscr{D}$ satisfies the equation

$$\begin{aligned} i\mathscr{D}_t + L\mathscr{D} = -\sqrt{2/(1+\beta)}\Bigg\{&cc^*\delta_0\begin{pmatrix}1\\-1\end{pmatrix} + c^2e^{2i\lambda_\beta t}\begin{pmatrix}\delta_1\\-\delta_2\end{pmatrix} \\ &+ c^{*2}e^{-2i\lambda_\beta t}\begin{pmatrix}\delta_2\\-\delta_1\end{pmatrix}\Bigg\}. \end{aligned} \tag{4.28}$$

We seek an inhomogeneous solution of (4.28) of the form

$$\mathscr{D}_p(x,t) = -\sqrt{2/(1+\beta)}\left\{cc^* d_0(x)\begin{pmatrix}1\\1\end{pmatrix} + c^2 d_1(x)e^{2i\lambda_\beta t} + c^{*2} d_2(x)e^{-2i\lambda_\beta t}\right\}, \tag{4.29}$$

where the scaler function $d_0$ and the vector functions $d_1$ and $d_2$ are the inhomogeneous solutions of the following equations

$$d_{0xx} - d_0 + 6\,\mathrm{sech}^2\, x d_0 = \delta_0, \tag{4.30}$$

$$Ld_1 - 2\lambda_\beta d_1 = \begin{pmatrix}\delta_1\\-\delta_2\end{pmatrix}, \tag{4.31}$$

$$Ld_2 + 2\lambda_\beta d_2 = \begin{pmatrix}\delta_2\\-\delta_1\end{pmatrix}. \tag{4.32}$$

Localized inhomogeneous solutions exist in Equation (4.30) since $\delta_0(x)$ is an even function in $x$ and the compatibility condition

$$\int_{-\infty}^{\infty} \delta_0\,\mathrm{sech}\, x \tanh x dx = 0 \tag{4.33}$$

is therefore satisfied. These solutions can be readily determined numerically. The solutions of (4.31) and (4.32) are a little bit more complicated. When $2\lambda_\beta > 1$, which happens when approximately $0.07 < \beta < 1$ (see Figure 4), the homogeneous equation of (4.31) has two linearly independent solutions $\psi(x,k)$ and $\psi(x,-k) = \psi^*(x,k)$ with $k^2 = 2\lambda_\beta - 1$. The compatibility condition for the existence of localized inhomogeneous solutions in (4.31) is

$$\int_{-\infty}^{\infty} \psi(x,k)^{\mathrm{T}} \sigma_3 \begin{pmatrix}\delta_1\\-\delta_2\end{pmatrix} dx = 0. \tag{4.34}$$

It can be checked numerically that this condition is never satisfied. The compatibility condition for Equation (4.32) can be readily found to be the same as (4.34) and is not satisfied either. This indicates that for $0.07 < \beta < 1$, all inhomogeneous solutions of Equations (4.31) and (4.32) are not localized. They always have oscillating tails at infinity. Therefore, given a localized initial condition $p_2(x,0)$ for Equation (4.26), those oscillating tails will be generated and spread out to infinity in the solution $p_2$. Due to this loss of energy, the linearly permanent oscillations in solution (4.22) with $p_1$ and $q_1$ as in (4.25) are not stable. The oscillational energy is gradually transferred into the outward-propagating oscillating tails, as is the case in the internal oscillations of degenerate vector solitons discussed in the previous subsection

(also see Figures 18 and 19). On the other hand, when $0 < 2\lambda_\beta < 1$, i.e., $0 < \beta < 0.07$, $2\lambda_\beta$ and $-2\lambda_\beta$ are no longer in the spectrum of the operator $L$. Therefore, the homogeneous equations of (4.31) and (4.32) have no bounded solutions. It follows that there is a unique localized solution $d_1(x)$ and $d_2(x)$ in Equation (4.31) and (4.32). It is then clear that a localized inhomogeneous solution $\mathscr{D}_p(x, t)$ of the form (4.29) can be constructed for Equation (4.28). The homogeneous solutions $\mathscr{D}_h(x, t)$ of (4.28) are a linear superposition of all the eigenmodes of the operator $L$ as determined in Section 3. When time is large, the continuous eigenmodes in $\mathscr{D}_h(x, t)$ disperse away as energy radiation so that only the inhomogeneous solution $\mathscr{D}_p(x, t)$ and the discrete eigenmodes of $L$ remain. These discrete eigenmodes can be absorbed into the vector soliton. When this is done the solution $\mathscr{D}(x, t)$ is left only with the localized solution $\mathscr{D}_p(x, t)$, which has a finite amount of energy. We can see now that only a small amount of energy will be transferred from the linearly permanent oscillations (terms up to order $\epsilon$ in (4.22)) into the order $\epsilon^2$ terms. Therefore, these linearly permanent oscillations will persist with only a little modification when terms up to second order in $\epsilon$ are considered in the solution (4.22). But it is easy to see that infinity-oscillating tails will appear sooner or later in the higher-order terms in (4.22) and the linearly permanent internal oscillations of vector solitons are always unstable. Of course, in these cases, the energy loss to oscillating tails will be even slower and these internal oscillations will sustain for a longer time.

Similar analysis can be carried out for an arbitrary single-hump vector soliton (2.1), and the results are qualitatively similar. Due to higher-order effects, the linearly permanent internal oscillations invariably generate infinity-oscillating tails, transfer energy into them, and gradually disappear. Recall that before the higher-order effects come into play, the linearization theory in Section 3 shows that the disturbed vector soliton will approach the state of permanent internal oscillations. It is then concluded that internal oscillations of vector solitons are never stable. They invariably emit energy to the far field and become weaker and weaker until they eventually disappear. The solution will asymptotically approach a single-hump vector soliton state.

## 5. Concluding remarks

The internal oscillations of vector solitons in birefringent nonlinear optical fibers is quite complicated in general. But by the linearization analysis, we clarified all the important features of those oscillations. We determined the discrete and continuous eigenmodes of the linearized equations around a single-hump vector soliton. We further identified the discrete eigenmodes that cause permanent internal oscillations to the vector soliton. These oscillations appear visually to be a combination of central position and width

oscillations in the $A$ and $B$ pulses. When higher-order effects are included, we found that the internal oscillations of vector solitons are always unstable. The oscillational energy is gradually transferred into the oscillating tails and is lost to the far field. But this energy transfer is usually very slow; therefore, the linearly permanent internal oscillations can sustain for a long time before they disappear. Eventually, the pulses undergoing internal oscillations will approach a single-hump vector soliton state, which is stable.

## References


1. A. Hasegawa and F. Tappert, Transmission of stationary nonlinear optical pulses in dispersive dielectric fibers, *Appl. Phys. Lett.* 23:142 (1973).
2. L. F. Mollenauer, R. H. Stolen, and J. P. Gordon, Experimental observation of picosecond pulse narrowing and solitons in optical fibers, *Phys. Rev. Lett.* 45:1045 (1980).
3. C. R. Menyuk, Nonlinear pulse propagation in birefringent optical fibers, *IEEE J. Quantum Electron* QE-23:174 (1987).
4. B. A. Malomed and S. Wabnitz, Soliton annihilation and fusion from resonant inelastic collisions in birefringent optical fibers, *Optim. Lett.* 16:1388 (1991).
5. J. Yang and D. J. Benney, Some properties of nonlinear wave systems, *Stud. Appl. Math.* 96:111 (1996).
6. T. Ueda and W. L. Kath, Dynamics of coupled solitons in nonlinear optical fibers, *Phys. Rev. A* 42:563 (1990).
7. V. K. Mesentsev and S. K. Turitsyn, Stability of vector solitons in optical fibers, *Optim. Lett.* 17:1497 (1992).
8. D. J. Kaup, B. A. Malomed, and R. S. Tasgal, Internal dynamics of a vector soliton in a nonlinear optical fiber, *Phys. Rev. E* 48:3049 (1993).
9. M. Haelterman and A. P. Sheppard, The elliptically polarized fundamental vector soliton of isotropic Kerr media, *Phys. Lett. A* 194:191 (1994).
10. Y. Silberberg and Y. Barad, Rotating vector solitary waves in isotropic fibers, *Optim. Lett.* 20:246 (1995).
11. N. N. Akhmediev, A. V. Buryak, J. M. Soto-Crespo, and D. R. Andersen, Phase-locked stationary soliton states in birefringent nonlinear optical fibers, *J. Optim. Soc. Am. B* 12:434 (1995).
12. D. J. Kaup, Perturbation theory for solitons in optical fibers, *Phys. Rev. A* 42:5689 (1990).
13. L. D. Landau and E. M. Lifshitz, *Quantum Mechanics*: *Non-relativistic Theory*, Pergamon Press, 1977.


The University of Vermont

(Received December 28, 1995)